PAPER

Check for updates

Fe₃O₄@WO₃-E-SMTU-Ni^{II}: as an environmentally-friendly, recoverable, durable and noble-free nanostructured catalyst for C–C bond formation reaction in green media†

Malihe Nayamadi Mahmoodabadi, [ID] Batool Akhlaghinia, [ID] * Sima Ein Afshar and Mostafa Safarzadeh

In the present study, Ni^{II} immobilized on Fe₃O₄@WO₃ functionalized by aminated epichlorohydrin using *S*-methylisothiourea (Fe₃O₄@WO₃-E-SMTU-Ni^{II}) as a novel magnetically separable nanostructured catalyst was successfully synthesized and characterized using FT-IR, XRD, TEM, FE-SEM, EDX, EDX mapping, VSM, TGA, H₂-TPR, ICP-OES and CHNS techniques. Characterization results revealed the spherical morphology and superparamagnetic behaviour of the as-synthesized catalyst with mean diameters of 19–31 nm as well as uniform distributions of the desired elements (Fe, O, W, C, N, S and Ni). The antibacterial activity of Fe₃O₄@WO₃-E-SMTU-Ni^{II} was evaluated against a set of Gram positive and Gram negative bacteria, and the catalyst showed considerable activity against the *Staphylococcus aureus* strain. The aforementioned nanostructured catalyst exhibited perfect catalytic efficiency in the Heck–Mizoroki and Suzuki–Miyaura reactions under mild conditions without using toxic solvents (EtOH as a green solvent and WEB as a benign base). Desired coupled products were obtained from the reaction of different Ar–X (X = I, Br, Cl) with alkyl acrylates and arylboronic acids. A high nickel content with negligible metal leaching during the course of reactions led to the high catalytic performance and stability of Fe₃O₄@WO₃-E-SMTU-Ni^{II} under optimized reaction conditions. The magnetically separation and ease of recovery and reusability of up to six cycles without a discernible decrease in catalytic activity or metal leaching are the most important features of the catalytic system from both industrial and environmental viewpoints.

1. Introduction

The carbon–carbon bond formation reaction as the cornerstone of organic chemistry has prevailed in the synthesis of a myriad of compounds. Using the C–C bond formation reaction, a wide range of complex organic molecules with various functional groups (drugs, heterocycles, agrochemicals, pharmaceutical intermediates and precursors) are synthesized under mild conditions.[1–4] The Heck–Mizoroki and Suzuki–Miyaura reactions (as the prominent approaches) are the most important and straightforward protocols used for the construction of C–C bonds in the presence of novel transition metal complexes, which can lead to important substituted olefins and biphenyls.[5–10] Palladium (based catalysts) as the first choice is still one of the most frequently investigated metals for cross-coupling reactions.[11] In modern organic synthesis, owing to

its limited resources, there is an urgent need to explore other more abundant, low cost and safer transition metal catalysts as alternatives to toxic, air sensitive and expensive precious metals, such as palladium, in C–C bond formation reactions. In this context, there has been a recent surge of interest for palladium-free conditions.[12] During the last two decades, nickel owing to its privileged catalytic behavior (such as availability of various oxidation states (Ni(0)–Ni(IV)), outstanding ability to coordinate to unsaturated molecules, facile oxidative addition and reductive elimination, homolytic Ni–C bond cleavage, exceptional reactivity of organonickel species,[13] as well as its inexpensive, non-toxic and abundant nature) has effectively participated in C–C bond formation reactions, and sometimes, the results are comparable to those with palladium.[14] Nowadays, nickel as a topic of discussion in catalytic approaches[13c,15] appears to be the most promising replacement for palladium as a catalyst.

Thus far, substantial progress has been made in the development of homogeneous Ni-based catalytic systems for Heck–Mizoroki and Suzuki–Miyaura reactions.[16] Some drawbacks, such as requiring a large amount of catalyst, difficulty in

Department of Chemistry, Faculty of Sciences, Ferdowsi University of Mashhad, Mashhad 9177948974, Iran. E-mail: akhlaghinia@um.ac.ir

separation of catalyst from the reaction mixture, recycling of catalyst and product contamination (as a serious problem in the pharmaceutical industry), could be regarded as the greatest barriers to the wider adoption of homogeneous catalytic systems. Considering the aforementioned limitations of the existing homogeneous catalysts, in addition to environmental and economical concerns, various attempts have been directed towards the development of heterogeneous Ni-based catalysts for Heck–Mizoroki and Suzuki–Miyaura reactions.[10,17] The heterogenization of Ni catalysts through the immobilization of homogeneous Ni catalysts on various solid supports has enhanced their catalytic activity and recyclability. Some of the novel heterogenized catalysts are primarily based on metal oxide supports, such as tungsten trioxide (WO_3). The WO_3 displays some advantageous properties, such as low cost, harmlessness, chemical inertness, stability in acidic and oxidative conditions and the fact that organic linkers can be robustly anchored to its surface, to provide catalytic centers.[18,19] The synthesis of nanostructured WO_3 with a wide range of applications in everyday life and in several research fields (from condensed matter physics to solid-state chemistry) as well as exceptionally versatile and unique characteristics (high specific surface area and good surface permeability) has become increasingly prominent.[20] To date, different heterogeneous catalysts based on WO_3 nanoparticles have been reported in some organic reactions, such as the oxidation of primary amines to oximes using WO_3/Al_2O_3;[21] oxidation of olefins, sulfides and cyclic ketones by WO_3/MCM-48;[22] syntheses of 1,8-dioxo-octahydroxanthene, tetrahydrobenzoxanthene and benzimidazolo quinazolinone derivatives in the presence of WO_3–SO_3H(WSA);[23] synthesis of alkyl levulinates from levulinic acid using WO_3-SBA-16;[24] preparation of WO_3@PdO core–shell nanospheres as a reusable catalyst in Heck–Mizoroki reaction;[25] synthesis of Fe_3O_4/WO_3 as a high-performance and recyclable visible-light photocatalyst;[26] water purification,[27] metathesis between ethene and 2-butene;[28] esterification of propionic acid;[29] photocatalytic activity,[30] NO_2 sensing,[31] photocatalytic O_2 production;[32] oxidation of cyclopentene to glutaraldehyde;[33] gas sensing properties[34] and adsorption of methylene blue from water.[35]

Presently, the major challenge of green chemistry is the separation procedure after the end of the reaction.[36] In this regard, the magnetic separation approach instead of conventional separation methods (centrifugation and filtration) is attractive owing to the facile separation of the catalyst from the reaction mixture using a simple magnetic bar.[37,38] The amazing advantages of magnetic heterogeneous catalysts are the elimination of cumbersome filtration and centrifugation procedures as well as the reduction of energy consumption, catalyst loss and processing time.[39]

Encouraged by our previous experiences to explore magnetic heterogeneous catalysts in the C–C bond formation reaction[40] and with respect to the importance of green chemistry legislation, Ni^{II} immobilized on Fe_3O_4@WO_3 functionalized by aminated epichlorohydrin with S-methylisothiourea (Fe_3O_4@WO_3-E-SMTU-Ni^{II}) was prepared, characterized and further examined for its catalytic activity in Heck–Mizoroki and Suzuki–Miyaura

reactions. The detailed synthetic procedures are discussed according to the synthetic process illustrated in Scheme 1. Fe_3O_4 NPs(I) were prepared by applying the co-precipitation method of Fe(III) and Fe(II) ions in an alkaline solution using a procedure reported in the literature.[41] To obtain Fe_3O_4@WO_3(II), Fe_3O_4 NPs were then coated by a WO_3 shell upon the reaction with WCl_6 and subsequent oxidation and calcination.[41] Then, functionalization of Fe_3O_4@WO_3 was carried out by suspending Fe_3O_4@WO_3 in pure epichlorohydrin at 60 °C with vigorous stirring to produce Fe_3O_4@WO_3 functionalized by epichlorohydrin (Fe_3O_4@WO_3-E) (III).[41] Thereafter, Fe_3O_4@WO_3 functionalized by aminated epichlorohydrin with S-methylisothiourea (Fe_3O_4@WO_3-E-SMTU) (IV) was obtained by the treatment of Fe_3O_4@WO_3-E with S-methylisothiourea hemisulfate salt in refluxing EtOH after 28 h.[42] Finally, immobilization of Ni^{II} was performed *via* the reaction of Fe_3O_4@WO_3-E-SMTU with an ethanolic solution of $NiCl_2 \cdot 6H_2O$ to afford Ni^{II} immobilized on Fe_3O_4@WO_3 functionalized by aminated epichlorohydrin with S-methylisothiourea (Fe_3O_4@WO_3-E-SMTU-Ni^{II}) (V).[43]

2. Experimental

2.1. General

All chemical reagents and solvents were purchased from Merck Chemical Companies and were used as received without further purification. The purity determinations of the products were
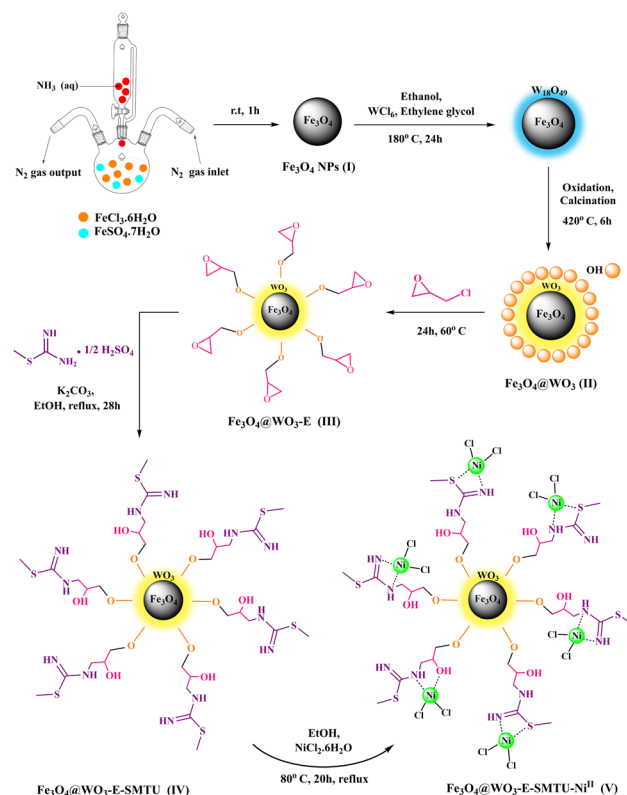
Scheme 1 Preparation steps of the Fe_3O_4@WO_3-E-SMTU-Ni^{II} nanostructured catalyst.

accomplished by TLC on silica gel polygram STL G/UV 254 plates. The melting points of the products were determined using an Electrothermal Type 9100 melting point apparatus. The pH was determined by applying an inoLab pH 7110 pH meter. The FT-IR spectra were recorded using an Avatar 370 FT-IR Thermo Nicolet spectrometer (Thermo Nicolet spectrometer, USA) at room temperature ranging from 4000 to 400 cm^{-1} with a resolution of 4 cm^{-1}. Elemental analyses were performed using a Thermo Finnegan Flash EA 1112 Series instrument. The NMR spectra were obtained using Brucker Avance 300, 400 and 500 MHz instruments in CDCl$_3$ and DMSO-d_6. Mass spectra were recorded using a CH7A Varianmat Bremem instrument at 70 eV electron impact ionization, in m/z (rel %). The crystalline structure of the catalyst was analyzed by XRD using a GNR Explorer Advance diffractometer with Cu Kα radiation ($\lambda = 1.54$ Å). Transmission electron microscopy (TEM) was performed using a Leo 912 AB microscope (Zeiss, Germany) with an accelerating voltage of 120 kV. FE-SEM images, EDX and EDX-mapping were recorded using a TESCAN, model: MIRA3 scanning electron microscope operating at an acceleration voltage of 30.0 kV and a resolution of about 200, 500 nm and 1 μm (manufactured in the Czech Republic). Thermogravimetric analysis (TGA) was carried out using an SDT Q600 Brochure Thermogravimetric Analyzer in the temperature range of 25–600 °C at a heating rate of 10 °C min^{-1} under air atmosphere. The magnetic properties of the catalyst were measured using a vibrating sample magnetometer (VSM, Magnetic Kavir Kashan Inst.). Hydrogen temperature-programmed reduction (H$_2$-TPR) was carried out using a Chemisorption Analyzer, NanoSORD, made by Sensiran Co., Iran. Inductively coupled plasma optical emission spectroscopy (ICP-OES) was carried out using Varian VISTA-PRO, CCD (Australia). The surface charge of the catalyst was determined using the CAD Zeta-potential instrument, the zeta compact model (France). UV-vis spectroscopy was recorded using a Nanodrop Array Spectrophotometer, Nano Ar 2015 model. The model Gram negative and Gram positive bacteria are *Escherichia coli* (ATCC 25922) and *Staphylococcus aureus* (ATCC 25923) strains, respectively. All yields refer to isolated products after purification by flash chromatography with silica gel.

2.2. Preparation of magnetic nanoparticles (Fe$_3$O$_4$ NPs) (I)

As mentioned in the literature, as nitrogen gas flows in a 500 mL three-necked round-bottom flask, FeCl$_2$·4H$_2$O (10 mmol, 1.99 g) and FeCl$_3$·6H$_2$O (12 mmol, 3.25 g) were completely dissolved in 30 mL deionized water at room temperature. Then, using a dropping funnel, NH$_4$OH solution (0.6 M, 200 mL) was added in a drop-wise manner to the above solution to reach the reaction pH of 11, as the black dispersion was vigorously stirred at room temperature. After 1 h, the resulting dispersion (named magnetic nanoparticles) was magnetically separated and washed thoroughly with deionized water until it was neutralized. After all, the Fe$_3$O$_4$ NPs(I) were dried at ambient temperature for 24 h.[41]

2.3. Preparation of Fe$_3$O$_4$@WO$_3$(II)

WCl$_6$ (0.5 mmol, 0.198 g), ethylene glycol (20 mL) and Fe$_3$O$_4$ magnetic nanoparticle (1.5 mmol, 0.346 g) were added to absolute ethanol (80 mL) under mild stirring. After 1 h, the resulting black suspension was transferred to a Teflon-lined autoclave, which was sealed and heated to 180 °C for 24 h, and then allowed to cool to room temperature. The obtained product (Fe$_3$O$_4$/W$_{18}$O$_{49}$ precursor) was collected magnetically, rinsed with absolute ethanol, and then dried at 70 °C for 1 h. Afterwards the final product was heated at 420 °C for 6 h to produce Fe$_3$O$_4$@WO$_3$(II).[41]

2.4. Preparation of Fe$_3$O$_4$@WO$_3$ functionalized by epichlorohydrin (Fe$_3$O$_4$@WO$_3$-E) (III)

Fe$_3$O$_4$@WO$_3$ functionalized by epichlorohydrin was prepared by the sonication of Fe$_3$O$_4$@WO$_3$(II) (0.7 g) in 6 mL pure epichlorohydrin for 30 min. The resultant suspension was heated at 60 °C with vigorous stirring. After 24 h, the resultant Fe$_3$O$_4$@WO$_3$ functionalized by epichlorohydrin (Fe$_3$O$_4$@WO$_3$-E) (III) was separated by an external magnet and washed with MeOH (5 × 10 mL) until an additional amount of epichlorohydrin was removed. Finally, the Fe$_3$O$_4$@WO$_3$-E(III) was dried at 40 °C under vacuum for 14 h.[41]

2.5. Preparation of Fe$_3$O$_4$@WO$_3$ functionalized by aminated epichlorohydrin with *S*-methylisothiourea (Fe$_3$O$_4$@WO$_3$-E-SMTU) (IV)

The obtained Fe$_3$O$_4$@WO$_3$-E(III) (1 g) was dispersed in ethanol (50 mL) for 30 min. Then, *S*-methylisothiourea hemisulfate salt (2.5 mmol, 0.347 g) and potassium carbonate (2.5 mmol, 0.345 g) were added to the reaction mixture and refluxed for 28 h. Subsequently, the resulting Fe$_3$O$_4$@WO$_3$ functionalized by aminated epichlorohydrin with *S*-methylisothiourea (Fe$_3$O$_4$@WO$_3$-E-SMTU) (IV) was magnetically separated and washed with ethanol (3 × 15 mL), before being dried at ambient temperature for 16 h.[42]

2.6. Preparation of Ni^{II} immobilized on Fe$_3$O$_4$@WO$_3$ functionalized by aminated epichlorohydrin with *S*-methylisothiourea (Fe$_3$O$_4$@WO$_3$-E-SMTU-Ni^{II}) (V)

The obtained Fe$_3$O$_4$@WO$_3$-E-SMTU(IV) (0.5 g) was dispersed in 25 mL ethanol by sonication for 20 min. Afterwards, NiCl$_2$·6H$_2$O (1 mmol, 0.257 g) was added to the resulting suspension at room temperature. Then, the reaction mixture was stirred at 80 °C for 20 h. Finally, Ni^{II} immobilized on Fe$_3$O$_4$@WO$_3$ functionalized by aminated epichlorohydrin with *S*-methylisothiourea (Fe$_3$O$_4$@WO$_3$-E-SMTU-Ni^{II}) (V) was magnetically separated, washed by ethanol and dried at room temperature.[43]

2.7. Preparation of WEB (water extract of banana peel ash)

WEB (Water Extract of Banana) (scientific name: *Musa balbisiana* Colla; family: Musaceae; species: *Musa balbisiana*) was obtained according to the previously reported method. Initially, the banana peels were washed and dried before burning them into ash. Therefore, the gained banana ash (5 g) was suspended in distilled H$_2$O (100 mL) and stirred for 10 min at room temperature. Finally, the resultant suspension was filtered through a sintered glass crucible. The filtrated product is

termed WEB. The pH meter was used to determine the pH of WEB, and it was found to be 9.8.[44]

2.8. Typical procedure for the Heck–Mizoroki reaction

To a mixture of methyl acrylate (1.2 mmol, 0.103 g), iodobenzene (1.0 mmol, 0.203 g) and WEB (water extract of banana peels ash) (1.0 mL) in EtOH (1 mL), $Fe_3O_4@WO_3$-E-SMTU-Ni^{II} (0.75 mol%, 0.01 g) was added. The resulting mixture was heated at 60 °C in an oil bath. After the completion of the reaction (45 min) monitored by TLC, the nanostructured catalyst was separated by a magnetic field, washed in turn with acetone (2 × 15 mL) and distilled water (4 × 15 mL). Then, the nanostructured catalyst was dried at 100 °C for 2 h and reused for a consecutive run under the same reaction conditions. The reaction mixture was then extracted with ethyl acetate (5 × 5 mL), and the combined organic layer was dried over anhydrous Na_2SO_4. After evaporation of the solvent, the crude product was purified by flash chromatography using *n*-hexane/ethyl acetate (8 : 2) as an eluent to afford the pure methyl cinnamate (0.153 g, % 95 yield).

2.9. Typical procedure for the Suzuki–Miyaura reaction

WEB (water extract of banana peel ash) (1.0 mL) was added to a mixture of iodobenzene (1.0 mmol, 0.203 g) and phenylboronic acid (1.2 mmol, 0.146 g) in EtOH (1 mL) at 60 °C. Then, $Fe_3O_4@WO_3$-E-SMTU-Ni^{II} (0.75 mol%, 0.01 g) was inserted into the resulting mixture under stirring. After the completion of the reaction (35 min) monitored by TLC, the nanostructured catalyst was separated by a magnetic field, washed in turn with acetone (2 × 15 mL) and distilled water (4 × 15 mL). The nanostructured catalyst was then dried at 100 °C for 2 h and reused for a consecutive run under the same reaction conditions. The reaction mixture was then extracted with ethyl acetate (5 × 5 mL), and the combined organic layer was dried over anhydrous Na_2SO_4. After evaporation of the solvent, the crude product was purified by flash chromatography using *n*-hexane/ethyl acetate (8 : 2) as an eluent to afford the pure 1,1′-biphenyl (0.145 g, % 95 yield).

2.10. Gram-scale procedure of the Heck–Mizoroki reaction

A flask was charged with a magnetic bead, methyl acrylate (60 mmol, 5.13 g), iodobenzene (50 mmol, 10.15 g), WEB (water extract of banana peels ash) (50 mL), EtOH (50 mL) and $Fe_3O_4@WO_3$-E-SMTU-Ni^{II} (38 mol%, 0.5 g). The resulting mixture was heated at 60 °C in an oil bath. After completion of the reaction (200 min) monitored by TLC, the nanostructured catalyst was separated using an external magnetic field. The reaction mixture was then extracted with ethyl acetate (5 × 250 mL), and the combined organic layer was dried over anhydrous Na_2SO_4. After evaporation of the solvent, the crude product was recrystallized with EtOH to afford pure methyl cinnamate.

2.11. Gram-scale procedure of the Suzuki–Miyaura reaction

To a mixture of iodobenzene (50 mmol, 10.15 g) and phenylboronic acid (60 mmol, 7.3 g) in EtOH (50 mL), WEB (water extract of banana peels ash) (50 mL) was added at 60 °C. Then,

$Fe_3O_4@WO_3$-E-SMTU-Ni^{II} (38 mol%, 0.5 g) was inserted into the resulting mixture under stirring. After completion of the reaction (3 h) monitored by TLC, the nanostructured catalyst was separated using an external magnetic field. The reaction mixture was then extracted with ethyl acetate (5 × 250 mL), and the combined organic layer was dried over anhydrous Na_2SO_4. After evaporation of the solvent, the crude product was purified by recrystallization from EtOH to afford pure 1,1′-biphenyl.

3. Results and discussion

3.1. Characterization of $Fe_3O_4@WO_3$-E-SMTU-Ni^{II}

The newly synthesized catalyst was entirely characterized through different techniques, such as Fourier transform infrared spectroscopy (FT-IR), X-ray diffraction (XRD), transmission electron microscopy (TEM), field emission scanning electron microscopy (FE-SEM), vibrating sample magnetometer (VSM), thermogravimetric analysis (TGA), hydrogen temperature-programmed reduction (H_2-TPR), inductively coupled plasma optical emission spectroscopy (ICP-OES) and elemental analysis (CHNS). It is noteworthy that the results derived from these techniques confirmed the successful preparation of the new nanostructured catalyst.

Moreover, the antibacterial activity of $Fe_3O_4@WO_3$-E-SMTU-Ni^{II} was studied by specifying the minimum inhibitory concentration (MIC), minimum bacterial concentration (MBC) and diameter inhibition zone (DIZ) against *Escherichia coli* (*E. coli*) and *Staphylococcus aureus* (*S. aureus*) bacteria (see ESI† file).

Fourier transform infrared (FT-IR) spectroscopy was employed to investigate the successful preparation of Fe_3O_4 NPs (a), $Fe_3O_4@WO_3$ (b), $Fe_3O_4@WO_3$-E (c), $Fe_3O_4@WO_3$-E-SMTU (d), and $Fe_3O_4@WO_3$-E-SMTU-Ni^{II} (e), and the obtained profiles are depicted in Fig. 1.
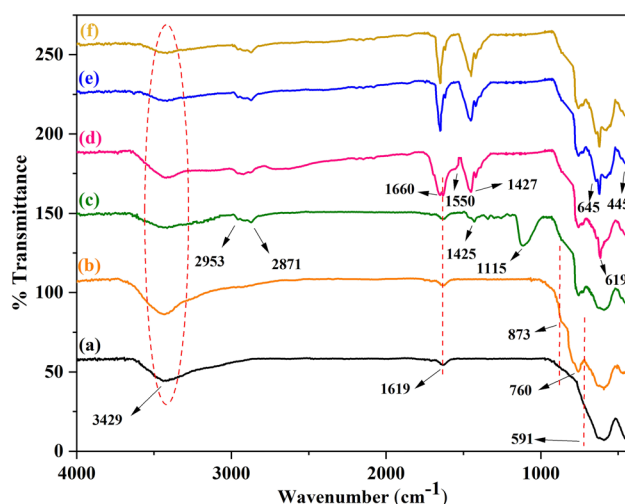
Fig. 1 FT-IR spectra of Fe_3O_4 NPs (a), $Fe_3O_4@WO_3$ core−shell (b), $Fe_3O_4@WO_3$-E (c), $Fe_3O_4@WO_3$-E-SMTU (d), $Fe_3O_4@WO_3$-E-SMTU-Ni^{II} (e) and the 6th reused $Fe_3O_4@WO_3$-E-SMTU-Ni^{II} from Suzuki–Miyaura reaction (f).

As shown in Fig. 1a, the absorption band related to the stretching vibration of the Fe–O bond in Fe_3O_4 appeared at 591 cm^{-1}. In addition, the absorption band at 1619 cm^{-1} and the broad band appearing at 3500–3100 cm^{-1} corresponded to the bending and stretching vibrations of the adsorbed water molecules and the surface-attached hydroxyl groups, respectively.[45]

The bands in the region of 1000–500 cm^{-1} can be attributed to the W–O (873 cm^{-1}) units and the stretching vibrations of the O–W–O (760 cm^{-1}) linkages (Fig. 1b).[46] The methylene C–H stretching and bending vibration at 2871, 2953 and 1425 cm^{-1} confirmed that the epoxy ring was attached to the $Fe_3O_4@WO_3$ framework. Moreover, the C–O–C vibrational stretching mode was visualized at 1115 cm^{-1} (Fig. 1c).[47]

The ring opening of the epoxy group with *S*-methylthiourea was proved through the existence of four new absorption bands at 1660, 1550, 1427 and 619 cm^{-1}. These four absorption bands can be assigned to the vibration of C=N (stretching), C–N (stretching), N–H (bending) and C–S (stretching) bonds, respectively (Fig. 1d).[42]

Absorption bands at 445 and 645 cm^{-1} demonstrate the coordination of Ni^{II} on $Fe_3O_4@WO_3$ functionalized by aminated epichlorohydrin with *S*-methylisothiourea, which is allocated to Ni–S and Ni–O vibrations, respectively.[48,49] Furthermore, the formation of metal–ligand bonds could be expressed by the coordination of Ni^{II} to the surface of the catalyst. This coordination could be authenticated by shifting the C=N (the stretching vibration band at 1660 cm^{-1}) and C–N stretching vibrations (positioned at 1550 cm^{-1}) toward the lower frequency.[50] Additionally, the intensities of –NH and probably –OH stretching frequencies decreased significantly owing to the coordination of Ni^{II} (Fig. 1e).

To distinguish the purity, phase, and crystallinity of the synthesized $Fe_3O_4@WO_3$-E-SMTU-Ni^{II}, XRD technique was employed (Fig. 2). The XRD pattern of Fe_3O_4 illustrated five characteristic reflection peaks at $2\theta = 62.4°$, 57.0°, 53.5°, 35.4° and 30.2°, which can be indexed to (4 4 0), (5 1 1), (4 2 2), (3 1 1), and (2 2 0) reflection planes of the crystalline magnetite with spinel structure, respectively.[51] As shown in Fig. 2b, the four primary diffraction peaks of $Fe_3O_4@WO_3$ situated at $2\theta =$ 22.84°, 23.9°, 28.56° and 33.34° were indexed to the (0 0 1), (2 0 0), (1 1 1) and (2 0 1) of tetragonal WO_3 (PDF no. 89-1287), respectively.[52] The XRD pattern of $Fe_3O_4@WO_3$-E-SMTU-Ni^{II} showed a sharp diffraction peak at around $2\theta = 45.8°$, which corresponded to the (1 1 1) reflection of Ni species.[53] Moreover, the average crystallite size of $Fe_3O_4@WO_3$-E-SMTU-Ni^{II} was estimated to be around 24 nm based on the Debye–Scherer equation ($D = K\lambda/\beta \cos\theta$).

Transmission electron microscopy (TEM) was utilized to investigate the size and morphology of $Fe_3O_4@WO_3$-E-SMTU-Ni^{II}. It can be easily deduced from the TEM image (Fig. 3a) that the as-synthesized catalyst has a spherical morphology with very satisfying monodispersity.

Furthermore, the distribution histogram of $Fe_3O_4@WO_3$-E-SMTU-Ni^{II} revealed that the average diameter of the nanoparticles was about 25 nm (Fig. 3b). The TEM results agreed well with the results obtained from XRD.

As can be observed in Fig. 4, field emission scanning electron microscopy (FE-SEM) was also performed to study the morphology of the as-synthesized catalyst. The FE-SEM images of $Fe_3O_4@WO_3$-E-SMTU-Ni^{II} exhibit spherical morphology with good dispersion.

The energy-dispersive X-ray (EDX) technique was applied to survey the types of elements present in the structure of $Fe_3O_4@WO_3$-E-SMTU-Ni^{II}. According to the data shown in
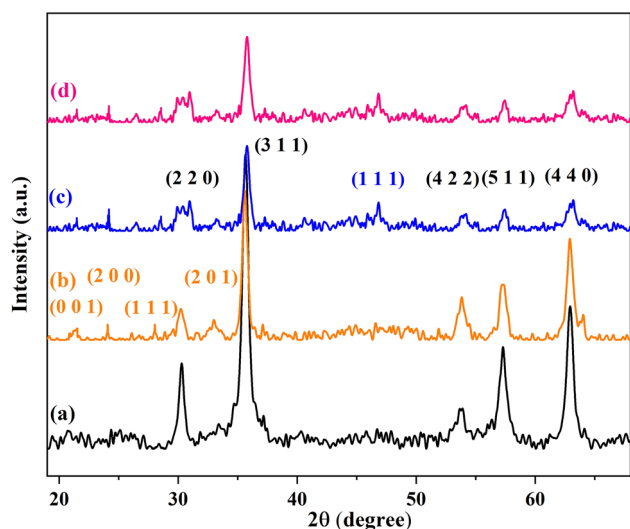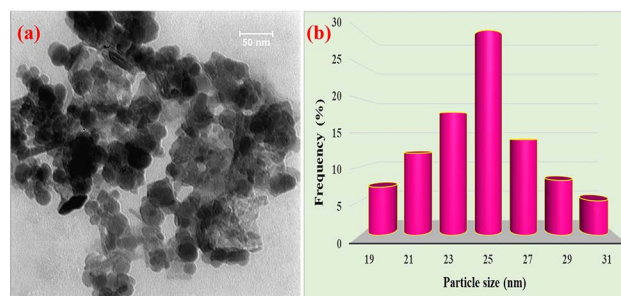

Fig. 3 TEM image of $Fe_3O_4@WO_3$-E-SMTU-Ni^{II} (a) and the particle size distribution histogram of $Fe_3O_4@WO_3$-E-SMTU-Ni^{II} (b).
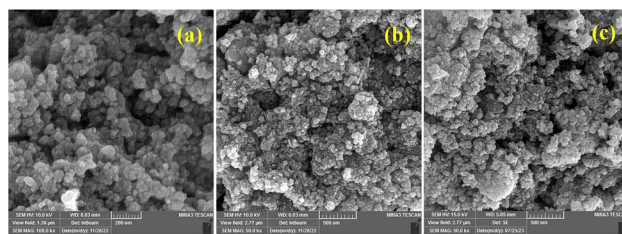

Fig. 2 XRD pattern of Fe_3O_4 NPs (a), $Fe_3O_4@WO_3$ (b), $Fe_3O_4@WO_3$-E-SMTU-Ni^{II} (c) and the 6th reused $Fe_3O_4@WO_3$-E-SMTU-Ni^{II} from Suzuki–Miyaura reaction (d).

Fig. 4 FE-SEM images of $Fe_3O_4@WO_3$-E-SMTU-Ni^{II} (a and b), and the 6th reused $Fe_3O_4@WO_3$-E-SMTU-Ni^{II} from Suzuki–Miyaura reaction (c).

Fig. 5a, the presence of Fe, O, W, C, N, S and Ni elements evidently confirmed the catalyst composition. Similarly, the considerable Ni^{II} intensity documented the successful immobilization of Ni^{II} on Fe_3O_4@WO_3-E-SMTU. Furthermore, EDX-mapping analysis was performed to evaluate the elemental composition on the surface of the nanostructured catalyst, as depicted in Fig. 5b. The presence of desired elements (Fe, O, W, C, N, S and Ni) with uniform distributions was affirmed.

The magnetic properties of Fe_3O_4@WO_3-E-SMTU-Ni^{II} were measured at ambient temperature using VSM. As illustrated in Fig. 6, the value of saturation magnetic moments of Fe_3O_4@WO_3-E-SMTU-Ni^{II} was Ms = 26 emu g^{-1}, which was lower than the reference value for Fe_3O_4 particles Ms = 57 emu g^{-1}.[54] The superparamagnetic behavior was preserved although the saturation magnetization of Fe_3O_4@WO_3-E-SMTU-Ni^{II} decreased after surface grafting. This can be attributed to the contribution of non-magnetic materials on the surface of the nanostructured catalyst.

The thermal stability of the Fe_3O_4@WO_3-E-SMTU-Ni^{II} was determined by thermogravimetric analysis (TGA). The results exhibited two weight losses in different temperature ranges. The TGA thermogram of the fresh catalyst in Fig. 7 demonstrated a significant weight loss of about 1.7% at temperatures below 200 °C, which could be attributed to the volatilization of residual water molecules and the ethanol solvent. Additionally,
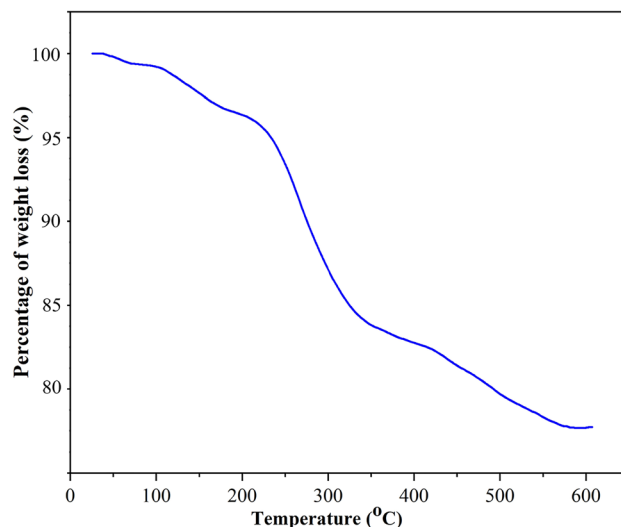

Fig. 7 TGA thermogram of Fe_3O_4@WO_3-E-SMTU-Ni^{II}.

the main weight loss (15.5%) ranging from 200 to 450 °C could be related to the removal of organic functional groups. The amount of organic motif supported on Fe_3O_4@WO_3 was estimated to be 0.70 mmol g^{-1}. These results agree well with the obtained elemental analysis data (N = 1.2%, C = 2.45% and S = 0.55%) and ICP-OES of the fresh catalyst. The ICP-OES analysis of the fresh catalyst indicated that 0.76 mmol of nickel was anchored on 1.00 g of the catalyst.

The type of Ni and W species present in the structure of Fe_3O_4@WO_3-E-SMTU was investigated by the hydrogen temperature-programmed reduction (H_2-TPR) technique. The H_2-TPR curves of Fe_3O_4@WO_3-E-SMTU-Ni^{II} (a) and the 6th reused Fe_3O_4@WO_3-E-SMTU-Ni^{II} from Suzuki–Miyaura reaction (b) are shown in Fig. 8. Two distinct reduction peaks are recognized in H_2-TPR profile in the range of 600–920 °C. The peak centered at 680 °C and the broad peak at higher

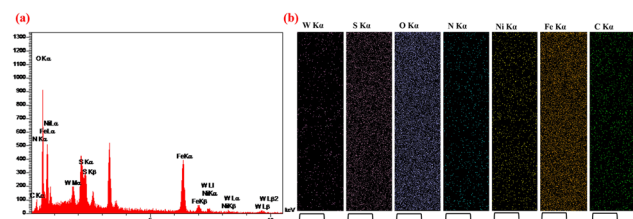Fig. 5 EDX spectrum of Fe_3O_4@WO_3-E-SMTU-Ni^{II} (a) and EDX-mapping analysis of Fe_3O_4@WO_3-E-SMTU-Ni^{II} (b).
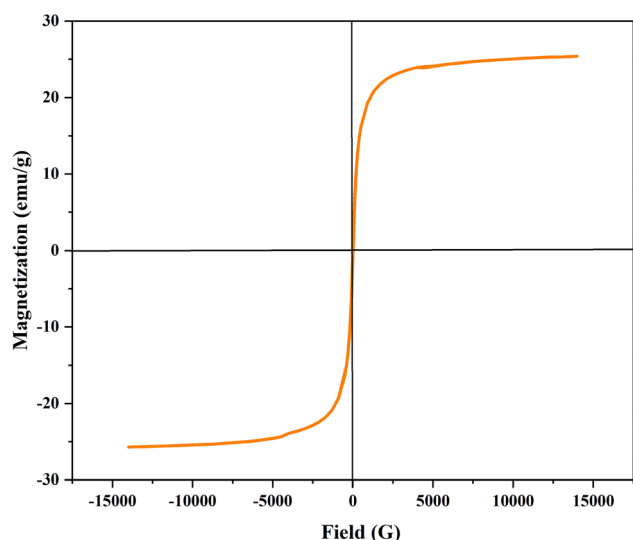
Fig. 6 Magnetization curve of Fe_3O_4@WO_3-E-SMTU-Ni^{II}.
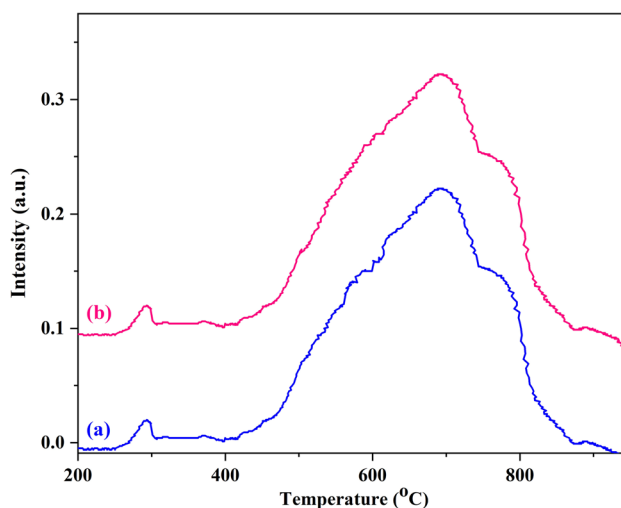
Fig. 8 H_2-TPR curves of Fe_3O_4@WO_3-E-SMTU-Ni^{II} (a) and the 6th reused Fe_3O_4@WO_3-E-SMTU-Ni^{II} from Suzuki–Miyaura reaction (b).

temperatures (720–920 °C) are related to the reduction in WO_3. The second reduction peak ranging from 200 °C to 400 °C may be attributed to the reduction in immobilized Ni^{II} to Ni^0.[55]

Interestingly, the same H_2-TPR profile was also observed for the 6th reused $Fe_3O_4@WO_3$-E-SMTU-Ni^{II} from Suzuki–Miyaura reaction.

R^1= H, 4-NO₂, 4-CN, 4-Cl, 4-CHO, 3-CHO, 4-OMe, 4-NH₂, 3-NH₂, 2-NH₂, 4-Me, 2-Thienyl
R^2= Me, Buⁿ
X= I, Br, Cl
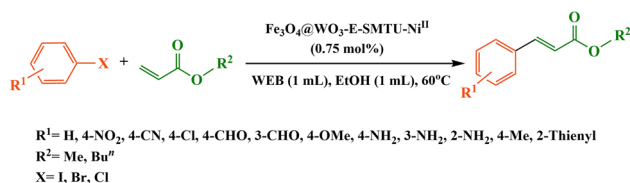
Scheme 2 Heck–Mizoroki reaction in the presence of the $Fe_3O_4@WO_3$-E-SMTU-Ni^{II} nanostructured catalyst.

R^1= H, 4-NO₂, 4-CN, 4-Cl, 4-CHO, 3-CHO, 4-OMe, 4-NH₂, 3-NH₂, 2-NH₂, 4-Me, 2-Thienyl
R^2= H, 4-Cl, 4-OMe
X= I, Br, Cl
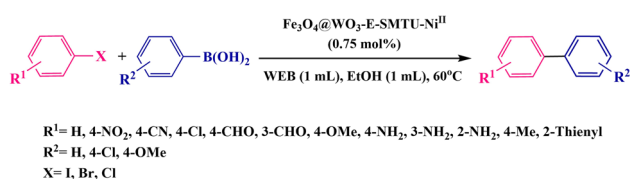
Scheme 3 Suzuki–Miyaura reaction in the presence of the $Fe_3O_4@WO_3$-E-SMTU-Ni^{II} nanostructured catalyst.

3.2. Catalytic performance of $Fe_3O_4@WO_3$-E-SMTU-Ni^{II} in carbon–carbon bond formation reactions

After the preparation and characterization of $Fe_3O_4@WO_3$-E-SMTU-Ni^{II}, its catalytic activity was investigated towards the C–C coupling reactions. Two important coupling reactions, namely, the Heck–Mizoroki and Suzuki–Miyaura reactions, were investigated using this nanostructured catalyst in green media (Schemes 2 and 3).

To identify the optimal conditions for the Heck–Mizoroki and Suzuki–Miyaura reactions, in preliminary experiments, the reactions of iodobenzene with methyl acrylate and phenylboronic acid were selected as model reactions (Tables 1 and 2). As performing the organic reaction in green media instead of using hazardous solvents is one of the important aspects of green chemistry,[56] the model reactions were initially conducted in EtOH. In the initial stages of the investigation, the model reactions were carried out without the catalyst and base. No

Table 1 Heck–Mizoroki reaction of iodobenzene with methyl acrylate in the presence of the $Fe_3O_4@WO_3$-E-SMTU-Ni^{II} nanostructured catalyst under different reaction conditions

Entry	Molar ratio of iodobenzene : methyl acrylate	Catalyst (mol%)	Base (mL)	Solvent (mL)	Temperature (°C)	Time (min)	Conversion (%)	Isolated yield (%)
1	1 : 1.2	—	—	1	60	24 (h)	0	0
2	1 : 1.2	—	1	1	60	24 (h)	0	0
3	1 : 1.2	0.75	—	1	60	24 (h)	0	0
4	**1 : 1.2**	**0.75**	**1**	**1**	**60**	**45**	**100**	**95**
5	1 : 1.2	0.7	1	1	60	55	100	90
6	1 : 1.2	0.6	1	1	60	55	100	90
7	1 : 1.2	0.5	1	1	60	65	100	82
8	1 : 1.2	0.85	1	1	60	45	100	95
9	1 : 1.2	0.75	1	1	80	30	100	92
10	1 : 1.2	0.75	1	1	Reflux	40	100	90
11	1 : 1.2	0.75	1	1	65	45	100	86
12	1 : 1.2	0.75	1	1	rt	24 (h)	62	48
13	1 : 1	0.75	1	1	60	60	100	85
14	1 : 1.3	0.75	1	1	60	45	100	95
15	1 : 1.2	0.75	0.5	1	60	65	100	72
16	1 : 1.2	0.75	1.5	1	60	45	100	85
17	1 : 1.2	0.75	1	—	60	24 (h)	35	30
18	1 : 1.2	0.75	1	0.5	60	65	100	70
19	1 : 1.2	0.75	1	1.5	60	40	100	90
20[a]	1 : 1.2	0.01 g	1	1	60	24 (h)	Trace	Trace
21[b]	1 : 1.2	0.01 g	1	1	60	24 (h)	10	Trace
22[c]	1 : 1.2	0.01 g	1	1	60	24 (h)	10	Trace
23[d]	1 : 1.2	0.01 g	1	1	60	24 (h)	21	18
24[e]	1 : 1.2	0.75	1	1	60	24 (h)	35	24

[a] Reaction was performed in the presence of Fe_3O_4 NPs. [b] Reaction was performed in the presence of $Fe_3O_4@WO_3$. [c] Reaction was performed in the presence of $Fe_3O_4@WO_3$-E. [d] Reaction was performed in the presence of $Fe_3O_4@WO_3$-E-SMTU. [e] Reaction was performed in the presence of $NiCl_2 \cdot 6H_2O$.

Table 2 Suzuki–Miyaura reaction of iodobenzene with phenylboronic acid in the presence of the $Fe_3O_4@WO_3$-E-SMTU-Ni^{II} nanostructured catalyst under different reaction conditions
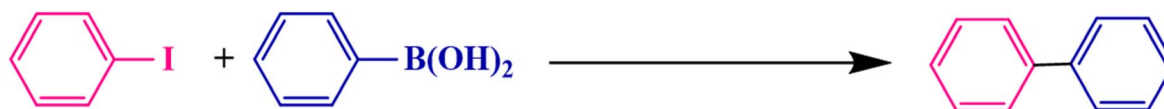
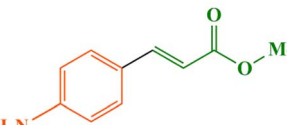| Entry	Molar ratio of iodobenzene : phenylboronic acid	Catalyst (mol%)	Base (mL)	Solvent (mL)	Temperature (°C)	Time (min)	Conversion (%)	Isolated yield (%)
1	1 : 1.1	—	—	1	60	24 (h)	0	0
2	1 : 1.1	—	1	1	60	24 (h)	0	0
3	1 : 1.1	0.75	—	1	60	24 (h)	0	0
4	**1 : 1.1**	**0.75**	**1**	**1**	**60**	**35**	**100**	**95**
5	1 : 1.1	0.7	1	1	60	50	100	85
6	1 : 1.1	0.6	1	1	60	75	100	80
7	1 : 1.1	0.5	1	1	60	90	100	72
8	1 : 1.1	0.85	1	1	60	35	100	95
9	1 : 1.1	0.75	1	1	80	21	100	93
10	1 : 1.1	0.75	1	1	Reflux	27	100	90
11	1 : 1.1	0.75	1	1	65	30	100	85
12	1 : 1.1	0.75	1	1	rt	24 (h)	60	45
13	1 : 1	0.75	1	1	60	50	100	87
14	1 : 1.3	0.75	1	1	60	35	100	95
15	1 : 1.1	0.75	0.5	1	60	55	100	75
16	1 : 1.1	0.75	1.5	1	60	30	100	81
17	1 : 1.1	0.75	1	—	60	24 (h)	40	35
18	1 : 1.1	0.75	1	0.5	60	60	100	78
19	1 : 1.1	0.75	1	1.5	60	35	100	95
20[a]	1 : 1.1	0.01 g	1	1	60	24 (h)	5	Trace
21[b]	1 : 1.1	0.01 g	1	1	60	24 (h)	10	Trace
22[c]	1 : 1.1	0.01 g	1	1	60	24 (h)	10	Trace
23[d]	1 : 1.1	0.01 g	1	1	60	24 (h)	17	10
24[e]	1 : 1.1	0.75	1	1	60	24 (h)	37	30
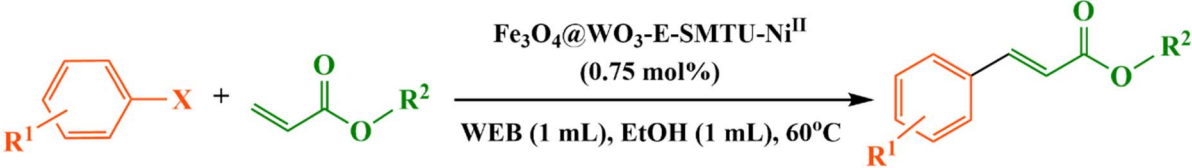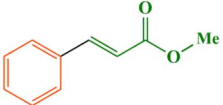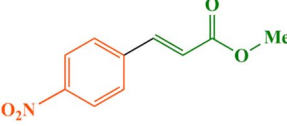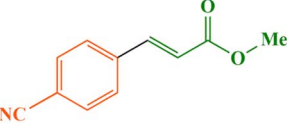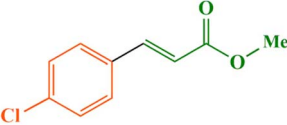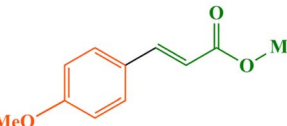
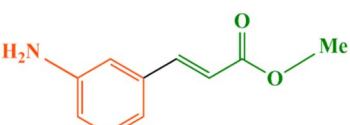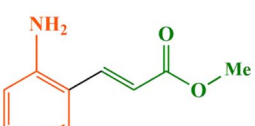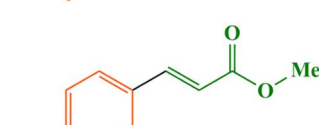[a] Reaction was performed in the presence of Fe_3O_4 NPs. [b] Reaction was performed in the presence of $Fe_3O_4@WO_3$. [c] Reaction was performed in the presence of $Fe_3O_4@WO_3$-E. [d] Reaction was performed in the presence of $Fe_3O_4@WO_3$-E-SMTU. [e] Reaction was performed in the presence of $NiCl_2 \cdot 6H_2O$.

products were observed after 24 h of running the reaction in EtOH at 60 °C (Table 1, entry 1 and Table 2, entry 1). From the economic and environmental viewpoints, continuing interest in using a safe, green, readily available and natural base has remained a significant challenge in C–C coupling reactions. Based on our previous reports[57] to reduce the environmental impacts, in this study, WEB (Water Extract of Banana ash) was prepared and used as a base in the Heck–Mizoroki and Suzuki–Miyaura reactions because of its basic behavior owing to the presence of sodium carbonate and potassium carbonate.[58] Interestingly, the model reactions did not produce the corresponding products by adding WEB (Water Extract of Banana ash) or $Fe_3O_4@WO_3$-E-SMTU-Ni^{II} to the reaction mixtures (Table 1, entries 2 and 3 and Table 2, entries 2 and 3). However, to our surprise, it was found that high yields of products were obtained in a short reaction time by performing the reactions in the presence of $Fe_3O_4@WO_3$-E-SMTU-Ni^{II} and using WEB as a base (Table 1, entry 4 and Table 2, entry 4). The results showed the essential role of the catalyst and base in proceeding with the Heck–Mizoroki and Suzuki–Miyaura reactions. Then, various amounts of catalyst loading were tested on the rates and yields

of the model reactions (Table 1, entries 4–8 and Table 2, entries 4–8). It was evident from Tables 1 and 2 that with 0.75 mol% of the catalyst, the highest yields of the desired products were obtained in a short reaction time. Decreasing of this amount to 0.7, 0.6 and 0.5 mol% afforded lower yields of the desired products, whereas additional amounts of the catalyst (0.85 mol%) were not significantly effective on the yields and rates of the reactions. This reaction also showed strong dependence on temperature (Table 1, entries 9–12 and Table 2, entries 9–12). Upon temperature examination, 60 °C proved to be the optimal reaction temperature. In surveying the best molar ratios of iodobenzene : methyl acrylate and iodobenzene : phenylboronic acid, it was found that the best results in the Heck–Mizoroki and Suzuki–Miyaura reactions were achieved by applying 1 : 1.2 and 1 : 1.1 molar ratios of iodobenzene : methyl acrylate and iodobenzene : phenylboronic acid, respectively (Table 1, entries 13, 14 and Table 2, entries 13, 14). Control experiments for the base-loading examinations listed in entry 15 and 16 indicated that base loading should be set using 1 mL of WEB. To determine the most optimal catalytic conditions, in the next screening experiments, the critical role

Table 3 Heck–Mizoroki reactions of different aryl halides with different olefins catalyzed by the $Fe_3O_4@WO_3$-E-SMTU-Ni^{II} nanostructured catalyst

Entry	R^1	X	R^2	Product	Time (min)	Conversion (%)	Isolated yield (%)
1	H	I	Me		45	100	95
2	4-NO$_2$	I	Me		30	100	95
3	4-CN	I	Me		35	100	96
4	4-Cl	I	Me		45	100	93
5	4-OMe	I	Me		60	100	95
6	4-NH$_2$	I	Me		110	100	94
7	3-NH$_2$	I	Me		115	100	90
8	2-NH$_2$	I	Me		135	100	90
9	4-Me	I	Me		65	100	90

Table 3 (*Contd.*)

Entry	R^1	X	R^2	Product	Time (min)	Conversion (%)	Isolated yield (%)
10	2-Thienyl	I	Me		80	100	92
11	H	Br	Me		110	100	93
12	4-NO$_2$	Br	Me		100	100	95
13	4-CN	Br	Me		95	100	94
14	4-Cl	Br	Me		90	100	95
15	4-CHO	Br	Me		165	100	92
16	3-CHO	Br	Me		195	100	90
17	4-OMe	Br	Me		3 (h)	100	97

Table 3 (*Contd.*)

Entry	R^1	X	R^2	Product	Time (min)	Conversion (%)	Isolated yield (%)
18	4-NH$_2$	Br	Me		3.5 (h)	100	90
19	3-NH$_2$	Br	Me		225	100	87
20	2-NH$_2$	Br	Me		4 (h)	100	85
21	H	Cl	Me		3.5 (h)	90	85
22	4-CN	Cl	Me		195	95	90
23	4-CHO	Cl	Me		4 (h)	85	75
24	4-NH$_2$	Cl	Me		7.5 (h)	85	70
25	2-NH$_2$	Cl	Me		10 (h)	80	70
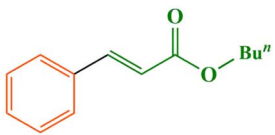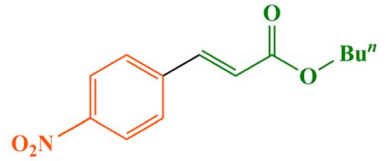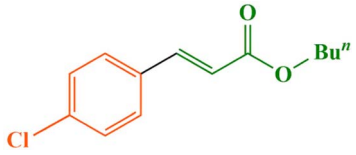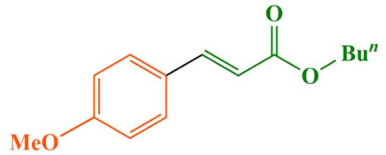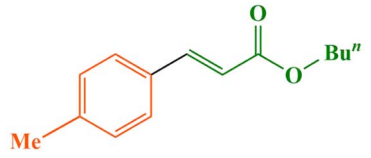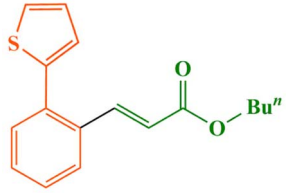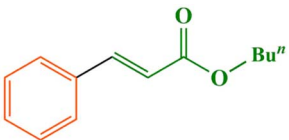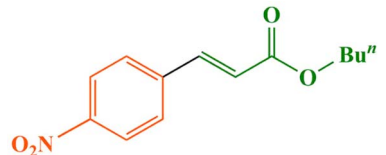
Table 3 (Contd.)

Entry	R^1	X	R^2	Product	Time (min)	Conversion (%)	Isolated yield (%)
26	H	I	Bu^n		35	98	95
27	4-NO$_2$	I	Bu^n		25	100	95
28	4-Cl	I	Bu^n		40	100	95
29	4-OMe	I	Bu^n		55	100	93
30	4-Me	I	Bu^n		50	100	92
31	2-Thienyl	I	Bu^n		60	100	90
32	H	Br	Bu^n		100	100	94
33	4-NO$_2$	Br	Bu^n		90	100	90

Table 3 (*Contd.*)

Entry	R^1	X	R^2	Product	Time (min)	Conversion (%)	Isolated yield (%)
34	4-CHO	Br	Bu^n		2 (h)	100	94
35	3-CHO	Br	Bu^n		2.5 (h)	100	90
36	4-OMe	Br	Bu^n		135	100	90
37	H	Cl	Bu^n		195	80	75
38	4-CN	Cl	Bu^n		185	95	85
39	4-CHO	Cl	Bu^n		220	75	70
40	4-NH_2	Cl	Bu^n		5.5 (h)	40	35
41	2-NH_2	Cl	Bu^n		6 (h)	30	25

Paper

Table 4 Suzuki–Miyaura reactions of different aryl halides with different arylboronic acids catalyzed by the $Fe_3O_4@WO_3$-E-SMTU-Ni^{II} nanostructured catalyst
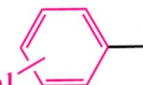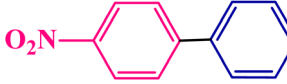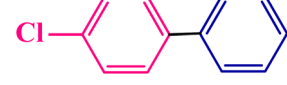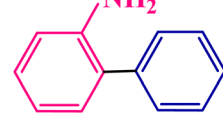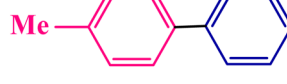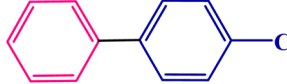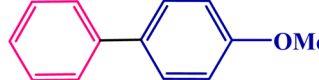
Entry	R^1	X	R^2	Product	Time (min)	Conversion (%)	Isolated yield (%)
1	H	I	H		35	100	95
2	4-NO_2	I	H		30	100	95
3	4-CN	I	H		32	100	95
4	4-Cl	I	H		30	100	93
5	4-OMe	I	H		75	100	90
6	4-NH_2	I	H		2 (h)	100	95
7	3-NH_2	I	H		125	100	96
8	2-NH_2	I	H		145	100	93
9	4-Me	I	H		55	100	93
10	2-Thienyl	I	H		85	100	93
11	H	I	4-Cl		30	100	95
12	H	I	4-OMe		52	100	92

Table 4   (Contd.)

Entry	R^1	X	R^2	Product	Time (min)	Conversion (%)	Isolated yield (%)
13	H	Br	H		55	100	95
14	4-NO$_2$	Br	H		40	100	95
15	4-CN	Br	H		50	100	92
16	4-Cl	Br	H		45	100	95
17	4-CHO	Br	H		75	100	92
18	3-CHO	Br	H		80	100	90
19	4-OMe	Br	H		170	100	90
20	4-NH$_2$	Br	H		195	100	92
21	3-NH$_2$	Br	H		225	87	81
22	2-NH$_2$	Br	H		4 (h)	100	95
23	H	Br	4-Cl		40	100	97
24	H	Br	4-OMe		65	100	92
25	H	Cl	H		3 (h)	90	85

Table 4 (*Contd.*)

Entry	R^1	X	R^2	Product	Time (min)	Conversion (%)	Isolated yield (%)
26	4-CN	Cl	H	NC—C6H4—C6H5	2.5 (h)	85	80
27	4-CHO	Cl	H	OHC—C6H4—C6H5	4 (h)	90	85
28	4-OMe	Cl	H	MeO—C6H4—C6H5	5 (h)	75	70
29	4-NH_2	Cl	H	H_2N—C6H4—C6H5	8 (h)	70	65
30	2-NH_2	Cl	H	2-NH_2-biphenyl	8.5 (h)	70	60

of EtOH was investigated in the model reaction (Table 1, entries 17–19 and Table 2, entries 17–19). Without using EtOH as a solvent, no reasonable yield of product was obtained even after a long time. After a few attempts, it was found that the best results of the Heck–Mizoroki and Suzuki–Miyaura reactions were obtained in the presence of Fe_3O_4@WO_3-E-SMTU-Ni^{II} (0.75 mol%) using WEB (1 mL) as a base in EtOH (1 mL) at 60 °C. To clarify the special catalytic activity of Fe_3O_4@WO_3-E-SMTU-Ni^{II} in the Heck–Mizoroki and Suzuki–Miyaura reactions in a set of experiments, the model reactions were carried out in the presence of Fe_3O_4 NPs, Fe_3O_4@WO_3, Fe_3O_4@WO_3-E, Fe_3O_4@WO_3-E-SMTU and $NiCl_2·6H_2O$ (Table 1, entries 20–24 and Table 2, entries 20–24). All of the cases were relatively insufficient for the coupling of iodobenzene using methyl acrylate and phenylboronic acid as benchmark reactions with observed conversion yields of trace and trace, 10% and trace, 10% and trace, 21% and 10% and 35% and 30% after 24 h, respectively.

After systematically evaluating the reaction parameters, we next proceeded to assess the scope of Heck–Mizoroki and Suzuki–Miyaura reactions of various aryl halides (containing electron-withdrawing or electron-donating groups) with different olefins and arylboronic acids in the presence of the as-synthesized nanostructured catalyst under optimized reaction conditions. The results are presented in Tables 3 and 4. As shown in Tables 3 and 4, owing to the lower C–I bond strength than the C–Br and C–Cl bonds, aryl iodides were coupled faster than aryl bromides and aryl chlorides.[59] (Table 3, entry 1 *vs.* entries 11 and 21 and Table 4, entry 1 *vs.* entries 13 and 25). Additionally, the high C–Cl and C–Br bond strength compared with the C–I bond slowed down the oxidative addition step in the Heck–Mizoroki and Suzuki–Miyaura reactions (see Scheme 4). However, it is evident that the optimized conditions were effective for the cross-coupling reactions of aryl bromide and aryl chloride to produce the desired products with good to moderate yields (Table 3, entries 11 and 21 and Table 4, entries 13 and 25).

Comparatively, aryl halides bearing electron-withdrawing groups at *para* positions produced target products more quickly than those containing electron-donating groups (Table 3, compare entries 2–4, 12–14, and 22 with 5–10, 17–20, and 24–25 and Table 4, compare entries 2–4, 14–16, and 26 with 5–10, 19–22 and 28–30). This means that the electron density of the aromatic ring essentially affects the elimination step of halide from the substrate (see Scheme 4). In addition, the sterically effects of *o*-substituted aryl halides in the Heck–Mizoroki and Suzuki–Miyaura reactions were studied under optimized reaction conditions. The longer reaction time and lower yields of corresponding products are observed in the case of *o*-substituted aryl halides compared to *p*-substituted ones, which is possibly owing to steric effects (Table 3, entry 6 *vs.* 8, entry 18 *vs.* 20 and entry 24 *vs.* 25 and entry 40 *vs.* 41 and Table 4, entry 6

Scheme 4 Proposed catalytic mechanism of the Heck–Mizoroki and Suzuki–Miyaura reactions catalysed by the Fe$_3$O$_4$@WO$_3$-E-SMTU-Ni^{II} nanostructured catalyst.

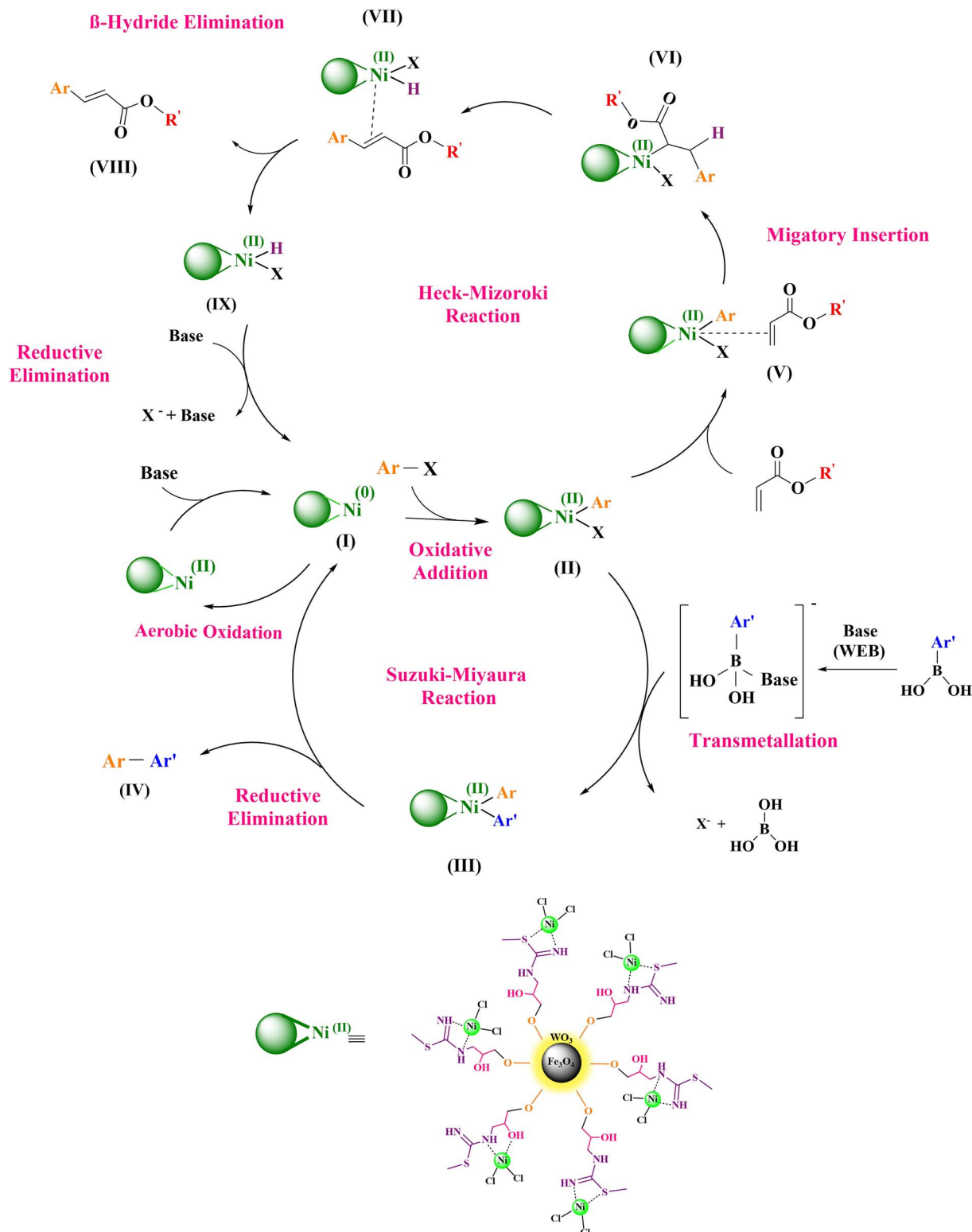*vs.* 8, entry 20 *vs.* 22 and entry 29 *vs.* 30). Furthermore, to confirm the generality of the present study, the reactivity of different olefins and different arylboronic acids was examined

in the Heck–Mizoroki and Suzuki–Miyaura reactions. Unsurprisingly, it is commonly believed that in the Heck–Mizoroki and Suzuki–Miyaura reactions, good catalytic activity and high

yields are achieved with methyl acrylate and *n*-butyl acrylate as well as phenylboronic acids endowed with electron-withdrawing or electron-donating substituents, respectively. A comparative study reveals that the reactions of *n*-butyl acrylate proceeded in a shorter reaction time with excellent yields than the reactions of methyl acrylate and phenylboronic acids with electron-withdrawing substituents (Table 3, entries 1, 11, 21 *vs.* 26, 32, 37 and Table 4 entries 1, 13 *vs.* 11, 23).

In addition, the chemoselectivity of the present method was investigated in Heck–Mizoroki and Suzuki–Miyaura reactions. Upon the cross-coupling reactions of 1-chloro-4-iodobenzene and 1-bromo-4-chlorobenzene (as dihalogenated aryl halides) with methyl acrylate and *n*-butyl acrylate and phenylboronic acid, exhibition of respective *m/z* values of the obtained products established the more reactivity of the C–I bond *vs.* C–Cl bond as well as the C–Br bond *vs.* C–Cl bond (Table 3, entries 4, 14 and 28 and Table 4, entries 4 and 16) (see ESI† file).

The progress of the Heck–Mizoroki and Suzuki–Miyaura reactions was monitored by the disappearance of the starting materials and the further formation of the desired products on TLC. All the desired products were known, isolated and purified by flash chromatography using silica gel as solid or oil products. The structure of the solid products was established by comparing their melting points with the reported values. Mass spectrometry exhibited their respective *m/z* values, and other useful fragmentation information confirmed the successful formation of some selected products. Furthermore, the structure of certain samples was effectively verified by surveying their high-field ^{1}H NMR and ^{13}C NMR spectral data (see ESI† file).

According to the ^{1}H NMR spectral data, the Heck–Mizoroki cross coupling reaction behaved in a stereospecific manner in the presence of Fe$_3$O$_4$@WO$_3$-E-SMTU-Ni^{II}, and in all the reactions, *E*-isomers were produced predominately. For instance, based on the ^{1}H NMR spectrum of methyl 3-(4-methoxyphenyl) acrylate (Fig. 9), the coupling constant (*J*) of H^a and H^b was estimated to be ~16 Hz, which is the characteristic of *E*-isomer (see ESI† file).

To elucidate the formation of the different products obtained from Heck–Mizoroki and Suzuki–Miyaura reactions in the presence of Fe$_3$O$_4$@WO$_3$-E-SMTU-Ni^{II}, through a comprehensive analogy of the previously reported mechanism in the literature[60] and our research, the following mechanisms are proposed in Scheme 4. The catalytic cycles started *via* an *in situ* reduction of Ni^{II} to Ni^0 species (I) in the presence of WEB (water extract of banana peel ash) as a base owing to the presence of sodium carbonate and potassium carbonate.[58,61] Then, the reaction was thought to continue by the oxidative addition of the aryl halide to Fe$_3$O$_4$@WO$_3$-E-SMTU-Ni^{II} producing intermediate II. Subsequently, the transmetalation of intermediate II with arylboronic acid in basic media led to the formation of intermediate III. Upon reductive elimination, the desired Suzuki–Miyaura product IV was obtained along with the regeneration of the active catalytic species for the next catalytic trial.

Moreover, the suggested mechanism of the Heck–Mizoroki reaction involves the addition of alkene to intermediate II through the formation of π-coordinated complex V, followed by the production of intermediate VI. Afterward, the desired Heck–
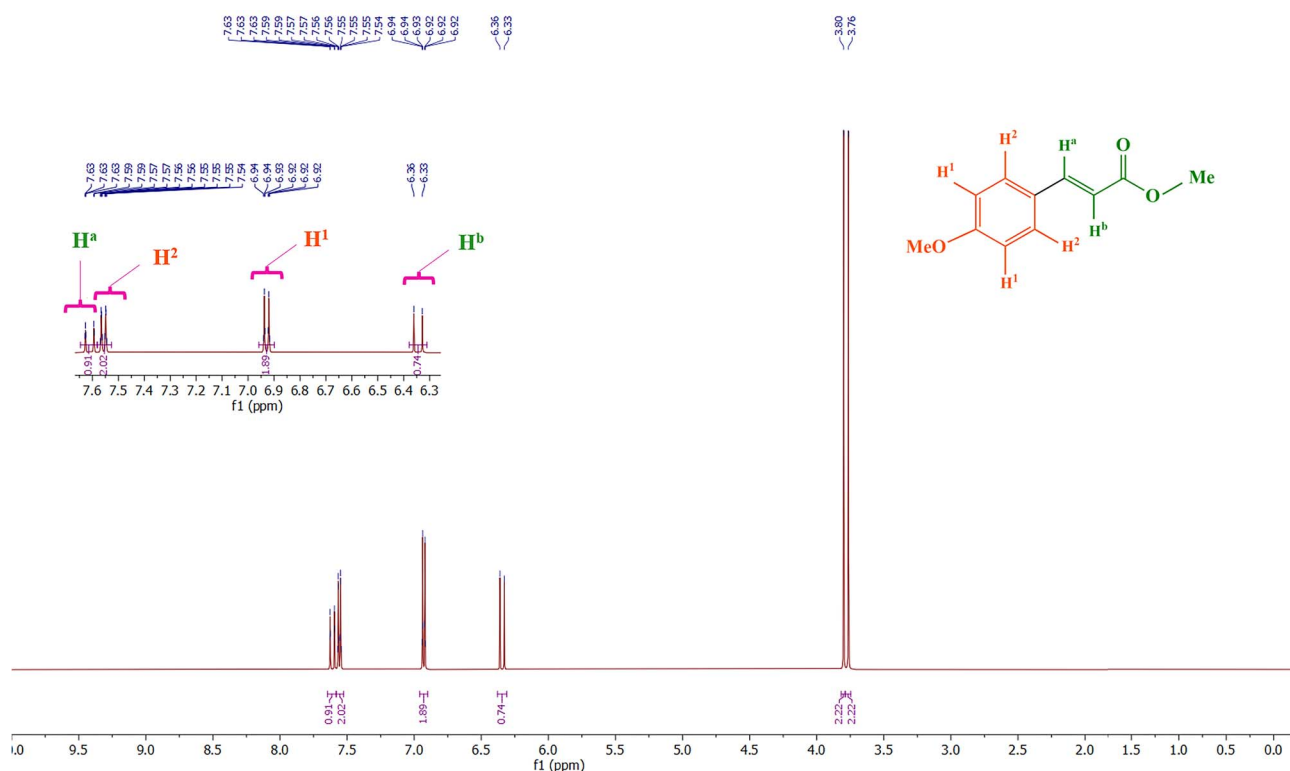

Fig. 9 ^{1}H NMR spectrum (300 MHz, CDCl$_3$) of methyl 3-(4-methoxyphenyl)acrylate.

Mizoroki product VIII was obtained upon β-hydride elimination of VII accompanied by the formation of IX. Then, the active catalytic species Ni^0(I) were produced for the next run upon the reductive elimination of intermediate IX in the presence of WEB.

Finally, Fe$_3$O$_4$@WO$_3$-E-SMTU-Ni^{II} was delivered to the reaction media *via* aerobic oxidation of the Ni^0 species (I) (based on the results of H$_2$-TPR in Fig. 8).[62] Further studies are underway in our laboratory to understand the mechanism of the Heck–Mizoroki and Suzuki–Miyaura reactions in the presence of Fe$_3$O$_4$@WO$_3$-E-SMTU-Ni^{II} in more detail.

The increasing interest in developing protocols and procedures, which motivates the industrial use of the synthesized catalyst, led to the study of a 50 gram-scale procedure for Heck–Mizoroki and Suzuki–Miyaura reactions. The experimental section demonstrated the detailed procedures, showing that Fe$_3$O$_4$@WO$_3$-E-SMTU-Ni^{II} exhibited superior catalytic activity compared to other catalysts and performed better in the synthesis and purification of the desired products.

In the field of heterogeneous catalysis, an essential question should be answered as to whether the catalyst is functioning in a heterogeneous manner or has a homogeneous behavior. To investigate the corresponding answer, a hot filtration test was conducted on Heck–Mizoroki and Suzuki–Miyaura model reactions under optimal conditions. Then, after half of the specified time of the Heck–Mizoroki and Suzuki–Miyaura model reactions passed (22 and 17 min), the nanostructured catalyst was removed from the reaction mixtures using an external magnetic field. Afterwards, the reactions were permitted to continue for further 22 and 17 min in the absence of a nanostructured catalyst. Thin layer chromatography was performed to track the progress of the reactions. There were no further coupling reactions even after an extended time. The ICP-OES analysis indicated that negligible amounts of active species (less than 0.08 and 0.08 mol%) leached out during the catalytic reactions. The strong attachment of nickel species to the surface of Fe$_3$O$_4$@WO$_3$-E-SMTU was evidently confirmed, which in turn established the heterogeneous nature of the nanostructured catalyst. The results of the hot filtration tests of the Heck–Mizoroki and Suzuki–Miyaura model reactions are presented in Fig. 10.

It is worth mentioning that the catalytic pathway may proceed through a "release-capture" mechanism. In other words, in many circumstances, leached and soluble metal species can be redeposited on the insoluble support during the hot filtration test.[63] Therefore, the negative hot-filtration test does not refer to the heterogeneous nature of the catalyst. To further elucidate the homogeneity/heterogeneity of the catalyst, poisoning tests were carried out on Heck–Mizoroki and Suzuki–Miyaura model reactions under optimized reaction conditions. Typical poisoning experiments were carried out with ethylenediamine tetraacetic acid (EDTA) as an effective Ni^{II} ion scavenger. EDTA with a high affinity to capture Ni^{II} ions formed the stable complex (X) (Scheme 5).[64] In four separate flasks, the Heck–Mizoroki and Suzuki–Miyaura model reactions were performed under optimized reaction conditions in the absence and presence of EDTA. TLC was performed to track the improvement in the reactions. The yields of the corresponding products of the Heck–Mizoroki and Suzuki–Miyaura model reactions were both 95% after 45 and 35 min, respectively. The time-dependent correlation of the product yields (Fig. 11) disclosed that EDTA did not considerably affect the improvement of the Heck–Mizoroki and Suzuki–Miyaura model reactions, and the reactions in the presence of EDTA were developed similar to that in the absence of it.

These observations mean that no leaching of Ni^{II} ions occurred in the reaction media during the entire course of the Heck–Mizoroki and Suzuki–Miyaura model reactions. Then, the true heterogeneous nature of the catalyst can be concluded from the obtained results. In other words, the reactions may be carried out on the surface of the Fe$_3$O$_4$@WO$_3$-E-SMTU-Ni^{II} nanostructured catalyst.
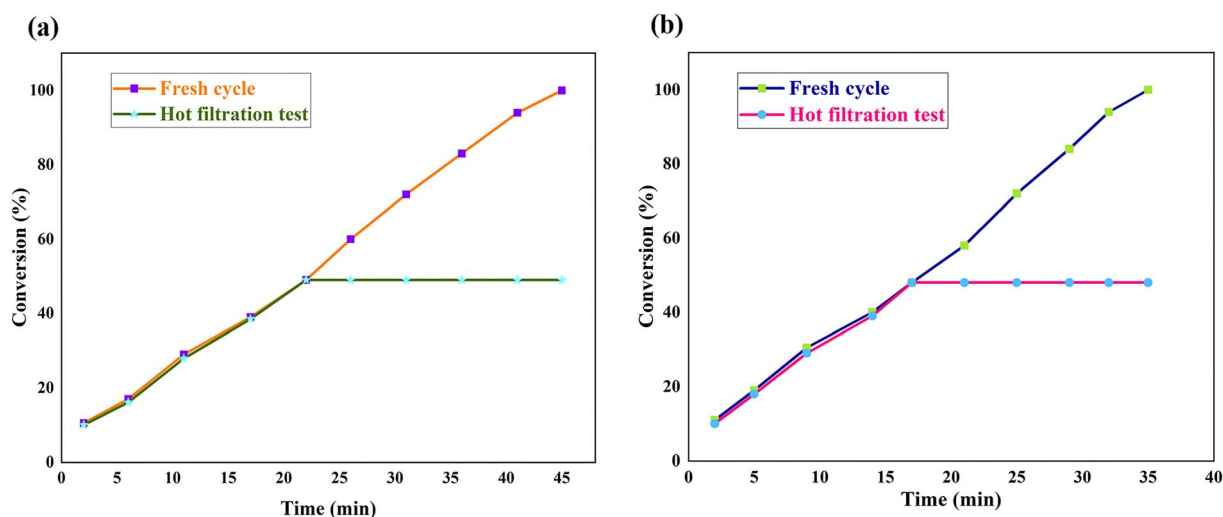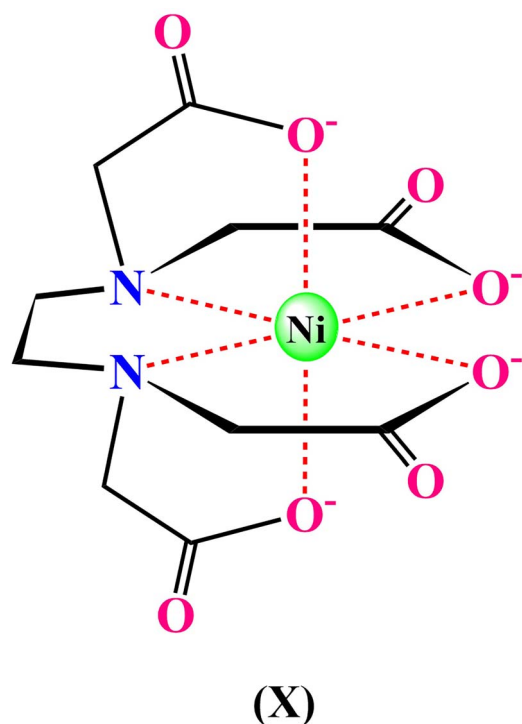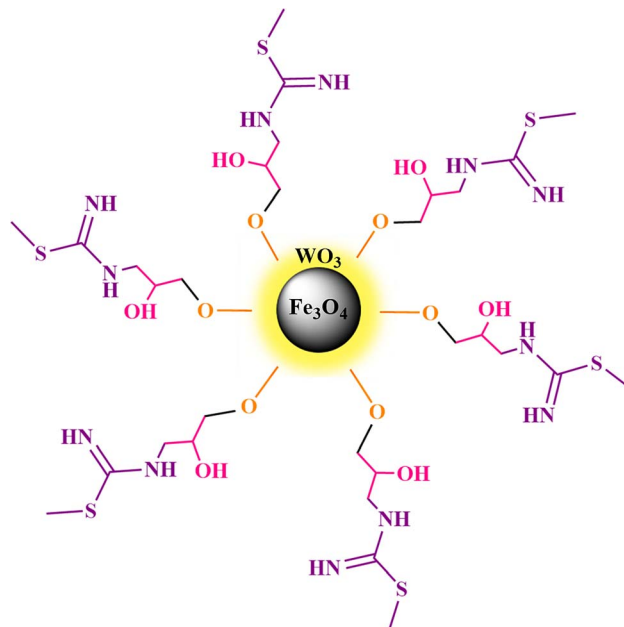

Fig. 10 Time-dependent correlation of the product yield in the reaction of iodobenzene with methyl acrylate (a) and phenylboronic acid (b) under optimized reaction conditions.

(X)

Scheme 5 Chemical structure of Ni^{II} EDTA complex (X).

Scheme 6 Chemical structure of Fe$_3$O$_4$@WO$_3$-E-SMTU.

Furthermore, to discern the homogeneity/heterogeneity of Fe$_3$O$_4$@WO$_3$-E-SMTU-Ni^{II}, the three-phase test was designed as a powerful technique that allows the nanostructured catalyst to be in its natural habitat. Then, the Suzuki–Miyaura model reaction was carried out in the absence and presence of Fe$_3$O$_4$@WO$_3$-E-SMTU as a strong scavenger to capture the homogeneous soluble nickel ions (Scheme 6). The reaction progress was followed by TLC, and the results are depicted in Fig. 12. Obviously, the reaction in the presence of Fe$_3$O$_4$@WO$_3$-

E-SMTU proceeded similarly to that in the absence of a scavenger. Based on the above observations, the presence of any soluble nickel ions in the reaction mixture was ruled out. Then, it can be deduced that the reaction possibly proceeded in a heterogeneous pathway.

Additionally, a kinetic study as another test (to investigate the possibility of the heterogeneous nature of Fe$_3$O$_4$@WO$_3$-E-SMTU-Ni^{II}) was performed on the Suzuki–Miyaura model reaction. Under optimized reaction conditions, the reaction yield and nickel leaching were measured during the reaction. During our studies, in four time intervals (15, 25, 35 and 45 min), the yield of the reaction was monitored by UV-vis spectroscopy
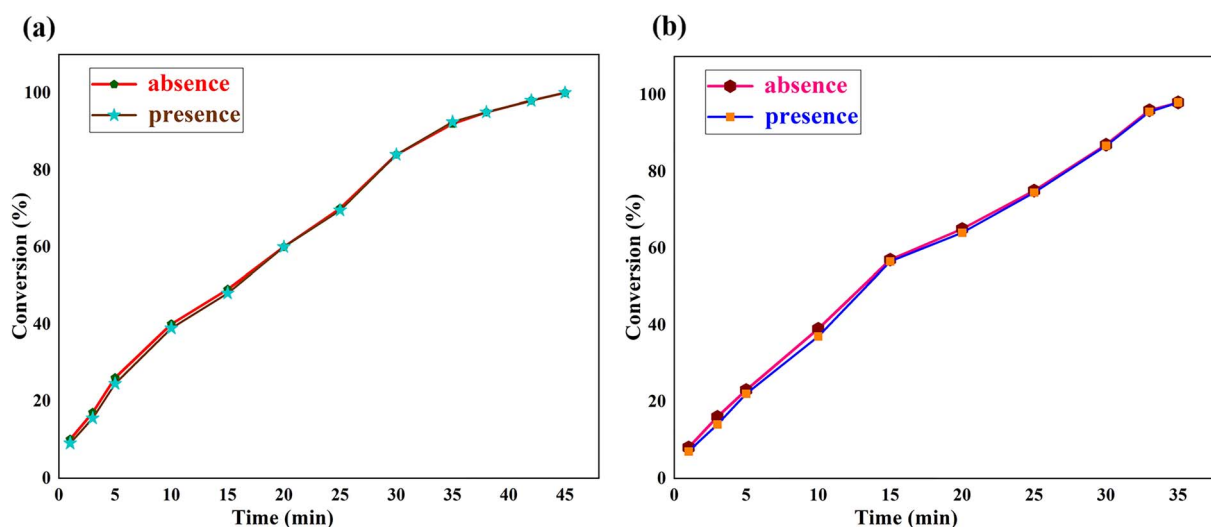

Fig. 11 Product yield of the reaction of iodobenzene with methyl acrylate (a) and phenylboronic acid (b) as a function of reaction time catalyzed by Fe$_3$O$_4$@WO$_3$-E-SMTU-Ni^{II} nanostructured catalyst in the absence and presence of EDTA.
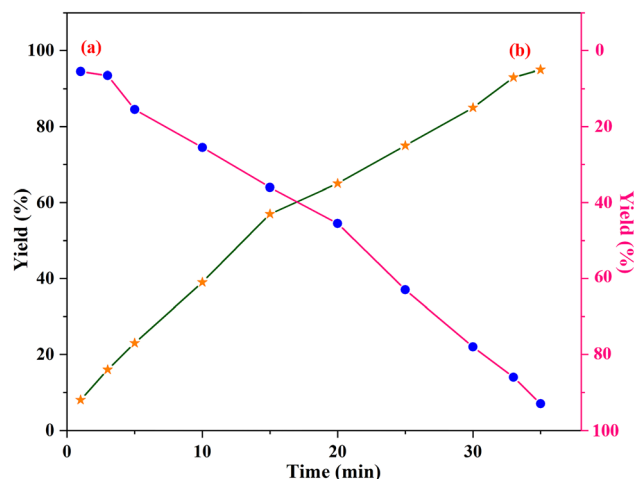
Fig. 12 Time-dependent correlation of the yield of Suzuki–Miyaura cross coupling reaction in the absence (a) and presence (b) of $Fe_3O_4@WO_3$-E-SMTU.

accompanied by determining the amount of leached nickel in the reaction mixture by applying ICP-OES techniques. The results are shown in Fig. 13. It is evident that after 15, 25, 35 and 45 min, the nickel concentrations (mol%) in solution/reaction yield (%) are 0.076/50, 0.079/82, 0.085/95 and 0.085/95, respectively. According to the obtained results, a negligible amount of nickel in solution cannot promote the reaction considerably, and any improvement in the reaction yield could be attributed to heterogeneous nickel species. Again, the heterogeneous nature of $Fe_3O_4@WO_3$-E-SMTU-Ni^{II} is proved according to the obtained results.

Finally, the results of all heterogeneity tests led us to conclude that $Fe_3O_4@WO_3$-E-SMTU-Ni^{II} with high catalytic activity under the described reaction conditions has a truly stable heterogeneous nature.

The crucial aspects of heterogeneous catalytic systems from a green chemistry viewpoint are recycling and recovery. In this
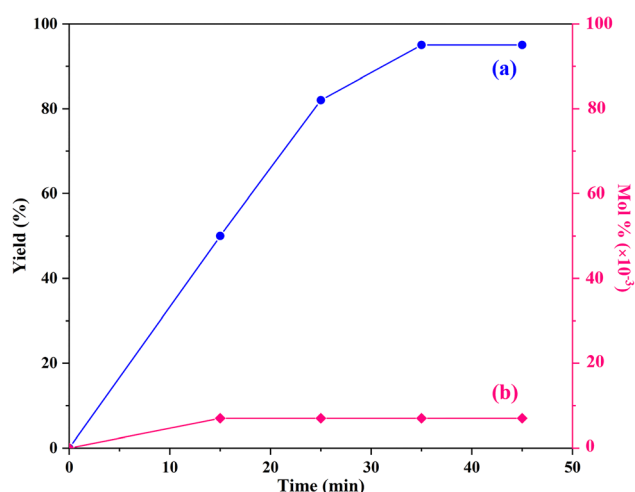
regard, the reusability of $Fe_3O_4@WO_3$-E-SMTU-Ni^{II} was next explored in the Heck–Mizoroki and Suzuki–Miyaura model reactions. At the end of each run, the reaction mixture was cooled to room temperature, and the nanostructured catalyst was simply separated by an external magnet, washed in turn with acetone (2 × 15 mL) and distilled water (4 × 15 mL) before drying at 100 °C for 2 h to be ready for re-employing directly in another fresh reaction mixture of both catalytic systems. It is evident from Tables 5 and 6 that a negligible decrease in the nanocatalyst activity occurred after six successive runs, which clearly demonstrated the high catalytic activity and stability of $Fe_3O_4@WO_3$-E-SMTU-Ni^{II} during the reaction cycles.

The turn over frequency (TOF) and turn over number (TON) of $Fe_3O_4@WO_3$-E-SMTU-Ni^{II} nanostructured catalyst were also calculated, and the results are shown in Tables 5 and 6. It is apparent from Tables 5 and 6 that the catalytic activity of the nanostructured catalyst did not significantly decrease even after 6 recycle runs from Heck–Mizoroki and Suzuki–Miyaura model reactions.

The Ni content of the freshly prepared $Fe_3O_4@WO_3$-E-SMTU-Ni^{II} nanostructured catalyst obtained using the ICP-OES technique was 0.76 mmol of Ni per 1.00 g of catalyst, while the ICP-OES analysis of the 6th recycled catalyst revealed that the recovered nanostructured catalyst from the reaction mixtures of the Heck–Mizoroki and Suzuki–Miyaura model reactions contained 0.73 and 0.71 mmol of Ni per 1.00 g of the nanostructured catalyst. The obtained results demonstrated that a negligible amount of nickel leached out from the surface of the nanostructured catalyst during the six runs of Heck–Mizoroki and Suzuki–Miyaura model reactions. The high stability along with the excellent catalytic performance of the present

Table 5 Reusability of $Fe_3O_4@WO_3$-E-SMTU-Ni^{II} nanostructured catalyst in the reaction of iodobenzene with methyl acrylate under the optimized reaction conditions

Entry	Time (min)	Conversion (%)	Isolated yield (%)	TOF (h^{-1})	TON
1	45	100	95	1.68	1.26
2	45	100	95	1.68	1.26
3	45	100	95	1.68	1.26
4	45/55	95/100	90/95	1.57/1.38	1.18/1.26
5	45/65	90/100	85/95	1.49/1.16	1.12/1.26
6	45/75	85/100	82/95	1.44/1	1.08/1.26

Table 6 Reusability of $Fe_3O_4@WO_3$-E-SMTU-Ni^{II} nanostructured catalyst in the reaction of iodobenzene with phenylboronic acid under the optimized reaction conditions

Entry	Time (min)	Conversion (%)	Isolated yield (%)	TOF (h^{-1})	TON
1	35	100	95	2.15	1.25
2	35	100	95	2.15	1.25
3	35	100	95	2.15	1.25
4	35/40	95/100	90/95	2.03/1.89	1.18/1.25
5	35/50	95/100	90/95	2.03/1.5	1.18/1.25
6	35/60	90/100	85/95	1.93/1	1.12/1.25

Fig. 13 Time-dependent correlation of yield (a) and nickel leaching (b) in the Suzuki–Miyaura model reaction.

© 2024 The Author(s). Published by the Royal Society of Chemistry

catalytic system may have originated from the strong coordination of nickel species to the ligands on the surface of $Fe_3O_4@WO_3$-E-SMTU.

Moreover, the 6th recovered $Fe_3O_4@WO_3$-E-SMTU-Ni[II] nanostructured catalyst from the Suzuki–Miyaura model reaction was characterized by FT-IR spectroscopy, XRD, FE-SEM and H_2-TPR techniques to gain deeper insight into the structural stability of the as-synthesized catalyst. The shapes, frequencies and relative intensities of the characteristic absorption bands in the FT-IR spectrum of the 6th recovered catalyst were entirely preserved (Fig. 1f). It is clearly obvious that no considerable changes occurred in the chemical structure and the hydrogen bonding network of the aforementioned catalyst after six recycle

runs. Additionally, it is important to note that no significant broadening or shifting occurred in the characteristic diffraction peaks of the 6th reused $Fe_3O_4@WO_3$-E-SMTU-Ni[II] compared to the fresh one (Fig. 2d). Interestingly, by comparing the FE-SEM images of the fresh $Fe_3O_4@WO_3$-E-SMTU-Ni[II] with the 6th recovered nanostructured catalyst, it could be concluded that no agglomeration occurred during the reusability of the $Fe_3O_4@WO_3$-E-SMTU-Ni[II] from the Suzuki–Miyaura model reaction (Fig. 4c). As can be inferred from H_2-TPR of the 6th recovered $Fe_3O_4@WO_3$-E-SMTU-Ni[II] (Fig. 8b), the oxidation state of Ni did not change even after 6 recycle runs.

Next, to examine the supremacy of the present synthetic procedures, model reactions of Heck–Mizoroki and Suzuki–

Table 7 Comparison of the catalytic activity of the $Fe_3O_4@WO_3$-E-SMTU-Ni[II] nanostructured catalyst with some literature precedents in the Heck–Mizoroki reaction[a]

Entry	Catalyst	mol%	Solvent	Base	Temperature (°C)	Time (h)	Yield (%)	Reusability	TOF (h^{-1})/TON	Ref.
1	Pd/CNTs[a]–PDA[b]	0.15	DMF	Et_3N	100	1	91.2	5	6.08/6.08	65
2	Fe_3O_4@TEA[c]–Pd	0.2	DMF	K_2CO_3	80	14 (min)	96	4	20.8/4.8	66
3	SWCNT–PAMAM[d]–Pd	0.1	DMF-H_2O	Et_3N	90	5	>99	6	1.98/9.9	67
4	Pd@CS[e]/PAAS[f]	5	DMAc	Et_3N	110	3	98	19	0.06/0.19	68
5	Co-IL[g]–MWCNT[h]	5	Toluene	$NaHSO_4$	100	3	77	6	0.05/0.15	69
6	Co-in-CNTs(II)	1	PEG	K_2CO_3	60	3	97	9	0.32/0.97	70
7	MNPs[i]@Cs–MS[j]–Co	1.1	PEG	K_3PO_4	80	1	88	5	0.8/0.8	71
8	MNP@PAMAM[k]–Co	0.55	DMF-H_2O	K_3PO_4	100	50 (min)	90	5	1.96/1.63	72
9	Fe_3O_4@boehmite–NH_2–Co[II]	0.44	H_2O	K_3PO_4	80	45 (min)	95	7	2.86/2.15	40a
10	Pd/NiCNTs–OH	10 mg	DMF	Et_3N	100	3	99.2	—	3.74/11.22	73
11	IL–Ni(II)–MNPs	0.12 g	DMF	Et_3N	100	4	98	5	—	74
12	Ni(II)–DABCO[l]@SiO_2	15 mg	DMF	Et_3N	100	3	97	6	—	10
13	Nano Ni	0.02 mmol	H_2O	K_2CO_3	140	16	81	6	—	75
14	$Fe_3O_4@WO_3$-E-SMTU-Ni[II]	0.75	EtOH	WEB	60	45 (min)	95	6	1.68/1.26	Present study

[a] Entry 13: reaction medium includes tetrabutylammonium bromide using a Teflon-lined stainless-steel autoclave. [a] Carbon nanotube. [b] Polydopamine. [c] Triethanolamine. [d] Single-walled carbon nanotube–polyamidoamine dendrimers hybrids. [e] Chitosan. [f] Sodium polyacrylate. [g] Ionic liquid. [h] Multiwall carbon nanotubes. [i] Magnetic (Fe_3O_4) nanoparticles. [j] Methyl salicylate. [k] Polyamidoamine. [l] 1,4-Diazabicy-cyclo[2.2.2] octane.

Table 8 Comparison of the catalytic activity of the $Fe_3O_4@WO_3$-E-SMTU-Ni[II] nanostructured catalyst with some literature precedents for Suzuki–Miyaura reaction

Entry	Catalyst	mol%	Solvent	Base	Temperature (°C)	Time (h)	Yield (%)	Reusability	TOF (h^{-1})/TON	Ref.
1	$CuNiFe_2O_4$ hollow spheres	0.01 g	EtOH–H_2O	K_2CO_3	80	50 (min)	95	9	—	76
2	Pd–Ni(0)[a]/RGO[b]	1.63 mg	EtOH–H_2O	NaOH	30	5	98	5	—	77
3	Pd_1Ni_4/CNF[c]	5 mg	EtOH–H_2O	K_2CO_3	80	1	98	10	7.86/7.86	78
4	Pd(II)–$NiFe_2O_4$	1	EtOH–H_2O	K_2CO_3	80	3	96	5	0.32/0.96	79
5	mTEG[d]-CS[e]-Co-Schiff-base	1	H_2O	K_2CO_3	90	1	93	6	0.93/0.93	80
6	G-Ni/Pd[f]	5 mg	DMF-H_2O	K_2CO_3	110	10 (min)	98	5	—	81
7	GO[g]/NiTAPP[h]	3	Dioxane	K_3PO_4	80	1	95	5	0.32/0.32	82
8	GO-Met[i]-Ni	2	Toluene	K_3PO_4	80	45 (min)	94	6	0.63/0.47	83
9	Pd–$CoFe_2O_4$	4 mg	EtOH	Na_2CO_3	Reflux	12	81	Multiple	—	84
10	Pd–Co/graphene	0.04 mmol	EtOH–H_2O	Na_2CO_3	80	2	96	5	—	85
11	Fe_3O_4@boehmite–NH_2–Co[II]	0.44	H_2O	KOH	80	30 (min)	95	7	4.3/2.15	40a
12	Fe_3O_4@SiO_2–EDTA–Ni(0)	1	EG	KOH	120	6	78	7	0.13/0.78	86
13	Fe_3O_4@SiO_2@mSiO_2–Pd(II)	1	EtOH	K_2CO_3	80	3	98	6	0.73/0.98	87
14	$Fe_3O_4@WO_3$-E-SMTU-Ni[II]	0.75	EtOH	WEB	60	35 (min)	95	6	2.15/1.26	Present study

[a] Ratio. [b] Ni_2O_3-around-Pd hybrid on graphene oxide. [c] Carbon nanofibers. [d] Mono-methoxytriethylene glycol. [e] Chitosan. [f] Ni/Pd core/shell nanoparticles supported on graphene. [g] Graphene oxide. [h] 5,10,15,20-Tetrakis(aminophenyl)porphyrin. [i] Metformin.

Miyaura reactions were compared with those of the other heterogeneous (Ni, Pd and Co based) catalysts reported in the literature. The results are summarized in Tables 7 and 8. The study encompassed an investigation of multiple factors: catalyst loading, solvent, type of base employed, temperature, reaction duration, reusability of the catalyst and catalytic activity. Although all the listed catalysts in Tables 7 and 8 afforded the desired products with their advantages, the current protocol is much superior to almost all of them in terms of catalyst loading (Table 7, entries 4–7 and 11 and Table 8, entries 4, 5, 7, 8, 12 and 13); non-toxic solvent (Table 7, entries 1–5, 8 and 10–12 and Table 8, entries 6–8); cost-effective and eco-friendly base (Table 7, entries 1–13 and Table 8, entries 1–13); the use of lower temperature (Table 7, entries 1–5 and 7–13 and Table 8, entries 1 and 3–13); lower reaction duration (Table 7, entries 1, 3–8 and 10–13 and Table 8, entries 1–5, 7–10, 12 and 13); the reusability of the catalyst, (Table 7, entries 1, 2, 7, 8 and 11 and Table 8, entries 2, 4, 6, 7 and 10) as well as better catalytic activity based on the corresponding turnover frequency (TOF) and turnover number (TON) results (Table 7, entries 4, 5, 6 and 7 and Table 8, entries 4, 5, 7, 8, 12 and 13).

Comparatively, among the other methods in Tables 7 and 8, the present investigations afforded truly mild processes using a simple separation procedure of $Fe_3O_4@WO_3$-E-SMTU-Ni^{II} nanostructured catalyst from the reaction mixture with an external magnetic field (Table 7, entries 1, 3–6, 10, 12 and 13 and Table 8, entries 2, 3, 5–8 and 10). Moreover, the outstanding use of an environmentally friendly base (WEB) and solvent is superior to previously reported methods.

4. Conclusion

In summary, Ni^{II} immobilized on $Fe_3O_4@WO_3$ functionalized by applying aminated epichlorohydrin with *S*-methyl-isothiourea ($Fe_3O_4@WO_3$-E-SMTU-Ni^{II}) was prepared as a novel, efficient and environmentally friendly heterogeneous nanostructured catalyst. The full characterization of $Fe_3O_4@WO_3$-E-SMTU-Ni^{II} was performed using various spectroscopic and microscopic techniques, such as FT-IR, XRD, TEM, FE-SEM, EDX, EDX mapping, VSM, TGA, H_2-TPR, ICP-OES and CHNS analyses. The characterization results confirmed the successful preparation of a nanostructured catalyst with spherical morphology, superparamagnetic behavior and mean diameters of 19–31 nm. The broth microdilution and disk diffusion methods confirmed the considerable antibacterial effect of the nanostructured catalyst. $Fe_3O_4@WO_3$-E-SMTU-Ni^{II} was found to show remarkable catalytic activity in the Heck–Mizoroki and Suzuki–Miyaura reactions using an eco-friendly and cost-effective base (WEB) in green media. A series of aryl iodides, bromides and chlorides (bearing electron-withdrawing and electron-donating substituents on different positions of aromatic rings) were coupled with alkyl acrylates and arylboronic acids to produce the corresponding products. Applying EtOH and WEB as green solvent and base, respectively, may be regarded as the predominant features supporting this synthetic method in a movement towards green chemistry. The nanostructured catalyst presented a high nickel content with

negligible metal leaching during the Heck–Mizoroki and Suzuki–Miyaura reactions. Unsurprisingly, $Fe_3O_4@WO_3$-E-SMTU-Ni^{II} can be easily recovered and reused for at least six cycles without deterioration in catalytic activity. Magnetic separation and an easy work-up procedure are other remarkable aspects of this methodology. Considering the aforementioned advantages, this method can be regarded as a practical alternative to other existing methods of C–C coupling reactions.

Author contributions

Malihe Nayamadi Mahmoodabadi: experimental investigation and visualization. Batool Akhlaghinia: supervision, writing, review, editing and funding acquisition. Sima Ein Afshar: experimental investigation. Mostafa Safarzadeh: experimental investigation.

Conflicts of interest

There are no conflicts to declare.

Acknowledgements

References

1 L. Rossi, N. Costa, J. Limberger and A. Monteiro, in *Nanocatalysts for the Suzuki Coupling Reactions. Nanocatalysis: Synthesis and Applications*, ed. V. Polshettiwar and T. Asefa, John Wiley & Sons, Inc., 2013, pp. 51–88.

2 A. Masarwa, D. Didier, T. Zabrodski, M. Schinkel, L. Ackermann and I. Marek, *Nature*, 2013, **505**, 199–203.

3 E. W. Werner, T. S. Mei, A. J. Burckle and M. S. Sigman, *Science*, 2012, **338**, 1455–1458.

4 V. Polshettiwar, A. Decottignies, C. Len and A. Fihri, *ChemSusChem*, 2010, **3**, 502–522.

5 A. Meijere, S. Brase and M. Oesterich, *Metal-Catalyzed Crosscoupling Reactions and More*, Wiley, Weinheim, 2014.

6 C. Bolm and M. Beller, *Transition Metals for Organic Synthesis*, Wiley-VCH Weinheim, 2004.

7 C. Torborg and M. Beller, *Adv. Synth. Catal.*, 2009, **351**, 3027–3043.

8 J. G. Vries, *Can. J. Chem.*, 2001, **79**, 1086–1092.

9 C. Wang, L. Salmon, R. Ciganda, L. Yates, S. Moya, J. Ruiz and D. Astruc, *Chem. Commun.*, 2017, **53**, 644–646.

10 A. R. Hajipour and P. Abolfathi, *Catal. Lett.*, 2017, **147**, 188–195.

11 (*a*) A. Suzuki, *Angew. Chem., Int. Ed.*, 2011, **50**, 6723–6737; (*b*) C. C. C. J. Seechurn, M. O. Kitching, T. J. Colacot and V. Snieckus, *Angew. Chem., Int. Ed.*, 2012, **51**, 5062–5085; (*c*) E. I. Negishi, *Angew. Chem., Int. Ed.*, 2011, **50**, 6738–6764; (*d*) N. Kambe, T. Iwasakia and J. Terao, *Chem. Soc. Rev.*, 2011, **40**, 4937–4947; (*e*) C. M. So and F. Y. Kwong, *Chem. Soc. Rev.*, 2011, **40**, 4963–4972; (*f*) B. Yuan, Y. Pan, Y. Li,

B. Yin and H. Jiang, *Angew. Chem., Int. Ed.*, 2010, **49**, 4054–4058; (*g*) Y. Li, X. M. Hong, D. M. Collard and M. A. E. Sayed, *Org. Lett.*, 2000, **2**, 2385–2388.

12 (*a*) R. Jana, T. P. Pathak and M. S. Sigman, *Chem. Rev.*, 2011, **111**, 1417–1492; (*b*) L. Zhang, Z. Zuo, X. Leng and Z. Huang, *Angew. Chem., Int. Ed.*, 2014, **53**, 2696–2700; (*c*) C. T. Yang, Z. Q. Zhang, Y. C. Liu and L. Liu, *Angew. Chem., Int. Ed.*, 2011, **50**, 3904–3907; (*d*) T. Hatakeyama, T. Hashimoto, K. K. A. D. S. Kathriarachchi, T. Zenmyo, H. Seike and M. Nakamura, *Angew. Chem., Int. Ed.*, 2012, **51**, 8834–8837.

13 (*a*) Y. Tamaru, Introductory Guide to Organonickel Chemistry, *Mod Org Chem.*, Wiley-VCH Verlag GmbH & Co. KGaA, 2005, pp. 1–40; (*b*) J. Montgomery, Organonickel Chemistry, in *Organometallics in Synthesis*, ed. B. H. Lipshutz, John Wiley & Sons, Inc., Hoboken, 2013, pp. 319–428; (*c*) S. Z. Tasker, E. A. Standley and T. F. Jamison, *Nature*, 2014, **509**, 299–309; (*d*) V. P. Ananikov, *ACS Catal.*, 2015, **5**, 1964–1971.

14 S. S. Wang and G. Y. Yang, *Catal. Sci. Technol.*, 2016, **6**, 2862–2876.

15 S. Bhakta and T. Ghosh, *Adv. Synth. Catal.*, 2020, **362**, 5257–5274.

16 (*a*) S. Pathan and A. Patel, *Dalton Trans.*, 2013, **42**, 11600–11606; (*b*) W. S. Zhang, D. W. Ji, Y. Li, X. X. Zhang, Y. K. Mei, B. Z. Chen and Q. A. Chen, *Nat. Commun.*, 2023, **14**, 651; (*c*) S. D. Ramgren, L. Hie, Y. Ye and N. K. Garg, *Org. Lett.*, 2013, **15**, 3950–3953; (*d*) V. Percec, G. M. Golding, J. Smidrkal and O. Weichold, *J. Org. Chem.*, 2004, **69**, 3447–3452.

17 (*a*) X. Wen, D. Tao, Z. Zhigang, L. Zhengxiu, C. Congmei, S. Wenjing and R. Maofei, *Appl. Catal., A*, 2020, **591**, 117405; (*b*) R. J. Key, J. M. M. Tengco, M. D. Smith and A. K. Vannucci, *Organometallics*, 2019, **38**, 2007–2014; (*c*) M. Binandeh, M. A. Nasseri and A. Allahresani, *Catalysts*, 2022, **12**, 976.

18 (*a*) K. Aravindraj and M. R. Selvaraj, *Synth. Commun.*, 2022, **52**, 1457–1476; (*b*) R. Ebrahimi, A. Maleki, Y. Zandsalimi and R. Ghanbari, *J. Ind. Eng. Chem.*, 2019, **73**, 297–305.

19 (*a*) X. Jiang, Y. Ding, S. Zheng, Y. Z. Ye, L. Li, J. Xu, X. Wang, J. Loh, E. Ye and L. Sun, *ChemSusChem*, 2022, **15**, e202102295; (*b*) A. H. Kianfar and M. A. Arayesh, *J. Environ. Chem. Eng.*, 2020, **8**, 103640.

20 Y. Yao, D. Sang, L. Zou, Q. Wang and C. Liu, *Nanomater*, 2021, **11**, 2136.

21 K. Suzuki, T. Watanabe and S. I. Murahashi, *J. Org. Chem.*, 2013, **78**, 2301–2310.

22 D. H. Koo, M. Kim and S. Chang, *Org. Lett.*, 2005, **7**, 5015–5018.

23 A. Amoozadeh and S. Rahmani, *J. Mol. Catal. A: Chem.*, 2015, **396**, 96–107.

24 S. S. Enumula, V. R. B. Gurram, R. R. Chada, D. R. Burri and S. R. R. Kamaraju, *J. Mol. Catal. A: Chem.*, 2017, **426**, 30–38.

25 M. Amini and A. Yousefi, *React. Kinet., Mech. Catal.*, 2016, **119**, 207–217.

26 G. Xi, B. Yue, J. Cao and J. Ye, *Chem.–Eur. J.*, 2011, **17**, 5145–5154.

27 M. A. Gondal, M. A. Dastageer and A. Khalil, *Catal. Commun.*, 2009, **11**, 214–219.

28 H. Liu, S. Huang, L. Zhang, S. Liu, W. Xin and L. Xu, *Catal. Commun.*, 2009, **10**, 544–548.

29 M. N. Alaya and M. A. Rabah, *Arabian J. Chem.*, 2017, **10**, 439–449.

30 Z. Lixia, Z. Qin and L. Qingcheng, *J. Rare Earths*, 2006, **24**, 60–66.

31 D. Menga, N. M. Shaalan, T. Yamazaki and T. Kikuta, *Sens. Actuators, B*, 2012, **169**, 113–120.

32 T. Peng, D. Ke, J. Xiao, L. Wang, J. Hu and L. Zan, *J. Solid State Chem.*, 2012, **194**, 250–256.

33 G. Lu, X. Li, Z. Qu, Q. Zhao, H. Li, Y. Shen and G. Chen, *Chem. Eng. J.*, 2010, **159**, 242–246.

34 Z. Wang, P. Sun, T. Yang, Y. Gao, X. Li, G. Lu and Y. Du, *Sens. Actuators, B*, 2013, **186**, 734–740.

35 J. Y. Luo, Z. Cao, F. Chen, L. Li, Y. R. Lin, B. W. Liang, Q. G. Zeng, M. Zhang, X. He and C. Li, *Appl. Surf. Sci.*, 2013, **287**, 270–275.

36 (*a*) A. Khojastehnezhad, M. Bakavoli, A. Javid, M. M. K. Siuki and F. Moeinpour, *Catal. Lett.*, 2019, **149**, 713–722; (*b*) A. Khojastehnezhad, A. Davoodnia, M. Bakavoli, N. Tavakoli-Hoseini and M. Zeinali-Dastmalbaf, *Chin. J. Chem.*, 2011, **29**, 297–302; (*c*) A. Khojastehnezhad, B. Maleki, B. Karrabi and E. R. Seresht, *Org. Prep. Proced. Int.*, 2017, **49**, 338–345.

37 Z. Dong, X. Le, C. Dong, W. Zhang and J. Ma, *Appl. Catal., B*, 2015, **162**, 372–380.

38 X. Cui, W. Zuo, M. Tian, Z. Dong and J. Ma, *J. Mol. Catal. A: Chem.*, 2016, **423**, 386–392.

39 L. M. Rossi, N. J. S. Costa, F. P. Silva and R. Wojcieszak, *Green Chem.*, 2014, **16**, 2906–2933.

40 (*a*) A. Mohammadinezhad and B. Akhlaghinia, *Green Chem.*, 2017, **19**, 5625–5641; (*b*) R. Jahanshahi and B. Akhlaghinia, *Catal. Lett.*, 2017, **147**, 2640–2655.

41 M. S. Ghasemzadeh and B. Akhlaghinia, *Bull. Chem. Soc. Jpn.*, 2017, **90**, 1119–1128.

42 R. Jahanshahi and B. Akhlaghinia, *New J. Chem.*, 2017, **41**, 7203–7219.

43 A. Ghorbani-Choghamarani, P. Moradi and B. Tahmasbi, *RSC Adv.*, 2016, **6**, 56458–56466.

44 P. R. Boruah, A. A. Ali, B. Saikia and D. Sarma, *Green Chem.*, 2015, **17**, 1442–1445.

45 M. H. Sayadi, S. Sobhani and H. Shekari, *J. Cleaner Prod.*, 2019, **232**, 127–136.

46 G. Xi, Y. Bing, C. Junyu and Y. Jinhua, *Chem.–Eur. J.*, 2011, **17**, 5145–5154.

47 F. Adam, K. M. Hello and H. Osman, *Chin. J. Chem.*, 2010, **28**, 2383–2388.

48 P. F. Yin, X. Y. Han, C. Zhou, C. H. Xia, C. L. Hu and L. L. Sun, *Int. J. Miner., Metall. Mater.*, 2015, **22**, 762–769.

49 F. Davar, Z. Fereshteh and M. Salavati-Niasari, *J. Alloys Compd.*, 2009, **476**, 797–801.

50 A. Ghorbani-Choghamarani, Z. Darvishnejad and B. Tahmasbi, *Inorg. Chim. Acta*, 2015, **435**, 223–231.

51 Y. Shao, J. Tao, T. Jingzhi and Z. Yongjie, *RSC Adv.*, 2015, **5**, 103943–103955.

52 P. Du, L. Yun, W. Yuncui, L. Can, D. Beibei, W. Yongqin, L. Linhui and Z. Bingsuo, *J. Alloys Compd.*, 2022, **893**, 162266.

53 M. Gopiraman, D. Dian, S. Somasundaram, I. M. Chung and I. S. Kim, *RSC Adv.*, 2018, **8**, 3014–3023.

54 G. Resende, G. V. S. Dutra, M. S. B. Neta, O. A. Araújo, S. B. Chaves and F. Machado, *Polym*, 2020, **12**, 2868.

55 N. Siddiqui, A. S. Roy, R. Goyal, R. Khatun, C. Pendem, A. N. Chokkapu, A. Bordoloi and R. Bal, *Sustain*, 2018, **2**, 191–198.

56 J. Safari, Z. Zarnegar and M. Heydarian, *J. Taibah Univ. Sci.*, 2013, **7**, 17–25.

57 (*a*) A. Allahi and B. Akhlaghinia, *Phosphorus, Sulfur Silicon Relat. Elem.*, 2020, **196**, 328–336; (*b*) M. Nayamadi Mahmoodabadi and B. Akhlaghinia, *Phosphorus, Sulfur Silicon Relat. Elem.*, 2023, **198**, 72–84.

58 D. C. Deka and N. N. Talukdar, *Indian Journal of Traditional Knowledge*, 2007, **6**, 72–78.

59 S. Rohani, G. Mohammadi Ziarani, A. Badiei, A. Ziarati, M. Jafari and A. Shayesteh, *Appl. Organomet. Chem.*, 2018, **32**, e4397.

60 R. M. Ansari, L. M. Kumar and B. R. Bhat, *Russ. J. Coord. Chem.*, 2018, **44**, 1–8.

61 X. Lei, K. A. Obregon and J. Alla, *Appl. Organomet. Chem.*, 2013, **27**, 419–424.

62 J. W. Xue, M. Zeng, S. Zhang, Z. Chen and G. Yin, *J. Org. Chem.*, 2019, **84**, 4179–4190.

63 B. Karimi, F. Mansouri and H. M. Mirzaei, *ChemCatChem*, 2015, 7, 1736–1789.

64 J. K. Nyborg and O. B. Peersen, *Biochem. J.*, 2004, **381**, e3.

65 Z. Luo, N. Wang, X. Pei, T. Dai, Z. Zhao, C. Chen, M. Ran and W. Sun, *J. Mater. Sci. Technol.*, 2021, **82**, 197–206.

66 A. Marandi and N. Koukabi, *Colloids Surf.*, 2021, **621**, 126597.

67 F. Giacalone, V. Campisciano, C. Calabrese, V. La Parola, Z. Syrgiannis, M. Prato and M. Gruttadauria, *ACS Nano*, 2016, **10**, 4627–4636.

68 Y. Du, S. Wei, M. Tang, M. Ye, H. Tao, C. Qi and L. Shao, *Appl. Organomet. Chem.*, 2020, **34**, e5619.

69 A. R. Hajipour, Z. Khorsandi and H. Karimi, *Appl. Organomet. Chem.*, 2015, **29**, 805–808.

70 A. R. Hajipour, Z. Khorsandi and H. Farrokhpour, *New J. Chem.*, 2019, **43**, 8215–8219.

71 A. R. Hajipour, F. Rezaei and Z. Khorsandi, *Green Chem.*, 2017, **19**, 1353–1361.

72 M. Arghan, N. Koukabi and E. Kolvari, *Appl. Organomet. Chem.*, 2019, **33**, e4823.

73 X. Wen, T. Dai, Z. Zhao, Z. Luo, C. Chen, W. Sun and M. Ran, *Appl. Catal., A*, 2020, **591**, 117405.

74 J. Safari and Z. Zarnegar, *C. R. Chim.*, 2013, **16**, 821–828.

75 W. Zhang, H. Qi, L. Li, X. Wang, J. Chen, K. Peng and Z. Wang, *Green Chem.*, 2009, **11**, 1194–1200.

76 M. Rajabzadeh, R. Khalifeh, H. Eshghi and M. Bakavoli, *J. Catal.*, 2018, **360**, 261–269.

77 R. Nie, J. Shi, W. Du and Z. Hou, *Appl. Catal., A*, 2014, **473**, 1–6.

78 G. Bao, J. Bai and C. Li, *Org. Chem. Front.*, 2019, **6**, 352–361.

79 A. S. Singh, R. S. Shelkar and J. M. Nagarkar, *Catal. Lett.*, 2015, **145**, 723–730.

80 S. Sobhani, H. H. Moghadam, J. Skibsted and J. M. Sansano, *Green Chem.*, 2020, **22**, 1353–1365.

81 Ö. Metin, S. F. Ho, C. Alp, H. Can, M. N. Mankin, M. S. Gültekin, M. Chi and S. Sun, *Nano Res.*, 2013, **6**, 10–18.

82 M. Keyhaniyan, A. Shiri, H. Eshghi and A. Khojastehnezhad, *New J. Chem.*, 2018, **42**, 19433–19441.

83 F. Raoufi, M. Monajjemi, H. Aghaei, K. Zare and M. Ghaedi, *ChemistrySelect*, 2020, **5**, 211–217.

84 K. K. Senapati, S. Roy, C. Borgohain and P. Phukan, *J. Mol. Catal. A: Chem.*, 2012, **352**, 128–134.

85 Y. S. Feng, X. Y. Lin, J. Hao and H. J. Xu, *Tetrahedron*, 2014, **70**, 5249–5253.

86 I. Dindarloo Inaloo, S. Majnooni, H. Eslahi and M. Esmaeilpour, *Appl. Organomet. Chem.*, 2020, **34**, e5662.

87 X. Le, Z. Dong, Z. Jin, Q. Wang and J. Ma, *Catal. Commun.*, 2014, **53**, 47–52.